Design of a Force-Controlled Cartilage Bioreactor

Final Report

FC Bioreactor
Jeffery Guo[1], Emilio Lim[2], Griffin Radtke[1], Sydney Therien[2]
Departments of Mechanical Engineering[1] and Biomedical Engineering[2]
Client: *Dr. Corinne Henak*
Advised by: *Dr. Corinne Henak* and *Dr. Paul Campagnola*
Teaching Assistant: *Patrick Dills*
University of Wisconsin – Madison
29 April 2024

Executive Summary

To help the Henak lab further study the disease progression of osteoarthritis, a bioreactor capable of mechanical loading is required to characterize the long-term metabolic impacts of cyclic loading on cartilage. This study aims to fill in the gap in literature where knowledge on disease progression over long timescales is limited. To accomplish this, a force-controlled bioreactor is designed with the ability to apply uniaxial cyclic loading within an incubator for a long timescale, intended to mimic what may be experienced *in vivo*.

The design of the bioreactor is split into two major components, the housing, and the actuation. The housing of the bioreactor will need to be able to withstand *in vivo* environment with consideration to temperature and humidity, fit within the incubator, and be autoclavable or able to withstand standard sanitation procedures. The final design of the bioreactor had dimensions of 11.5” by 8.5” by 8.3”, using a mix of different materials to suit the needs of different sections. The prototype of the bioreactor is made with a polylactic acid (PLA) base, acrylic panels, polytetrafluoroethylene (PTFE) compressive pillars, and a PLA sample tray with six 35-mm diameter wells.

The actuation of the bioreactor is controlled by a VC125C/M voice coil actuator (VCA) sourced from ThorLabs. The actuation team tested three different circuits to determine which circuit design is best suited to achieve the desired force. The target of the actuation is to produce a force of approximately 5.5N, equating (via Hookean relations) to approximately 20% strain, at a physiological triangular wave profile of 0.5Hz to 10Hz. To accomplish this force profile, the voice coil needs to be supplied with 6V at 0.7A. Ultimately, the team decided to use an NMOS transistor circuit which comprises an NMOS transistor, microcontroller, power supply, diode, and resistors. The microcontroller intended to be used in the Henak lab is the NI DAQ which will be responsible for generating the input wave profile. The output voltage that drives the voice coil actuator will be directly controlled by the power supply.

In summary, the final prototype is able to function appropriately for single-sample experimentation in the Henak lab. Future works could include fabricating the bioreactor housing out of aluminum, so the entire housing is autoclavable. Other components such as the linear bearings, voice coil actuator, NI DAQ, and circuitry would also need to be purchased to scale up testing to six samples. The bioreactor will help provide a key insight into how osteoarthritis progresses and potentially finding a better way of tackling this problem.

Table of Contents

Introduction

An estimated half billion individuals worldwide live with osteoarthritis (OA), causing significant detriment to quality of life and over $100 billion in annual direct & indirect costs [1]. While its expression varies, OA is often simplified as a general degradation of articular cartilage, although it is more properly understood as a biochemical alteration in synovial joint tissue. While symptom-based treatment for the disease is commonplace, treatment for the condition itself, due to its inherent complexity, is far beyond the current scientific horizon. That mentioned complexity arises from the variety of signaling pathways involved in OA progression—in the context of this report, we will focus on cartilage metabolism, or redox balance, as a specific agent in OA [2].

Literature has identified cartilage redox balance, synonymous in the context/scope of this work with metabolism, as a potential cause for OA. Metabolic dysregulation—or imbalance in the reliance on energy-producing cellular pathways (i.e., glycolysis & oxidative phosphorylation)—is common in many disease types. Nonetheless, the causative agents of this imbalance in redox state within the context of OA are little understood [3], [4], [5].

Our client, Dr. Henak, an Assistant Professor in the Department of Mechanical Engineering and her lab, in part, investigate the relationship between cartilage metabolism and disease state. Recent work both within her lab and the literature has postulated mechanical loading as this causative agent, with loading inducing metabolic dysfunction and OA-esque damage [6], [7]. Further, this dysfunction has been demonstrated as a time-dependent phenomena. Past work, however, has been limited to small timescales (i.e., less than one hour), thereby clearly necessitating a method by which to apply these mechanical insults over greater periods of time (i.e., several days to several weeks) [6]. Herein lies the primary focus of this project—to capture the full picture of cartilage metabolic dysfunction and its relation to OA, Dr. Henak seeks to investigate this balance over greater timescales.

From that research focus arose the problem statement and overall client need for this project. That is, to characterize the long-term relation between mechanical loading, cartilage metabolism, and cartilage disease state, the Henak Lab requires a bioreactor to apply a controlled, cyclic, uniaxial compressive stress to articular cartilage samples over long (i.e., hours, days, or weeks) timescales, as depicted within **Figure 1**. With that general client need comes several design specifications, briefly described below and more comprehensively discussed in the design specification table in **Appendix A**:

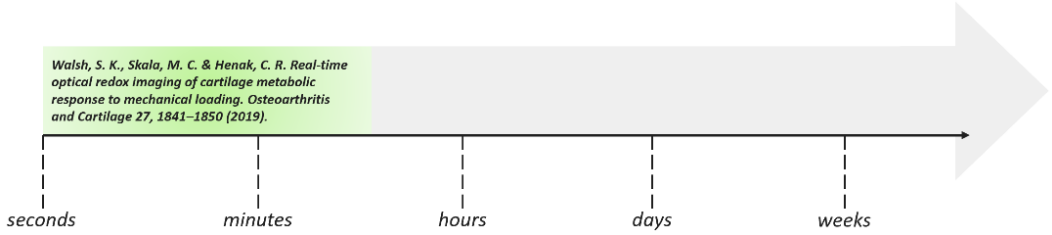

Figure 1. The Henak Lab has characterized the relationship between cartilage metabolic balance and loading on short timescales; the cartilage bioreactor is intended to fill this remaining timescale gap.

Broadly, the bioreactor must meet three characteristic requirements: that is, it must apply the desired forces, must be incubator-compatible, and must remain within the allotted budget of

$5000. Regarding the first, the client requires that the force output be both force-controlled (i.e., to avoid creep-related sample liftoff arising from the poroelastic nature of cartilage) and capable of outputting sufficient force to induce approximately 20% uniaxial compressive engineering strain, that the force profile – as previously mentioned – is cyclic with a triangular or sinusoidal profile (i.e., with a frequency of 0.1 – 10 Hz) to approximate in vivo loading, and that the material in contact with the cartilage (i.e., when in compression) is both low-friction and biocompatible. The second requirement is more straightforward: simply, the bioreactor must fit within the Henak Lab's incubator (20 x 21 x 25 in^3), operate within the incubator (i.e., humid and at 37° C), and capable of biosafety-relevant sanitation procedures (e.g., autoclave, UV, general ethanol cleansing, etc.) to avoid culture contamination.

Prior to addressing this semester's work, however, it is necessary to first discuss design guidance. Our design approach, both fall and spring semester, took inspiration from the literature as well as industry. For instance, prior work has been done in the field of tissue engineering to design a cartilage bioreactor comparable to the needs of our client, providing useful insight into potential conceptual designs, as depicted within **Figure 2** [8]. Work in industry likewise heavily informed design, as referenced in **Appendix E**. It should be noted, however, that review of work in industry was less relevant, as no device capable of applying the client's need for force-controlled, uniaxial compressive stress was found. Two manufacturers of tissue culture-based bioreactors capable of applying cyclic mechanical loading were identified: FlexCell (**Appendix E**; **Figure 3**) and CellScale [9]. Both, however, in their compressive bioreactor systems, rely on either hydrostatic actuation (i.e., not uniaxial) or displacement control, thereby failing to meet client specifications. Further, while no standards were applied directly over the course of the semester's work, standards guiding the overall biocompatibility of tissue culture-related devices, such ASTM F813-20, should be considered for future work.

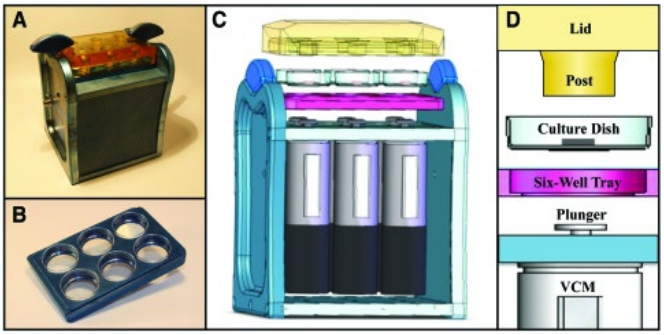

Figure 2. Prior work provides inspiration for the overall schematic build of a force-controlled cartilage bioreactor [5].

With those design criteria and supporting/competing designs considered, work then proceeded on more applicable overall conceptualization and design. Work for the semester, as before, was subdivided into two sub-teams – housing and circuitry – with each taking strides to deliver a final prototype meeting client specifications by the semester's end. Here, we outline this final work, as well as the supporting design decisions and engineering logic applied to reach that stage.

Overview of the Final Bioreactor Architecture

Building off the foundation of the fall semester (**Appendix E**) and implementing week-to-week guidance via client meetings, work proceeded on the development of a final housing prototype as well as a functioning, more refined controlling circuit. Several prototypes, both analytical (**Figure 3**) and physical, were considered, with general design iteration, engineering calculation, and hands-on work used to arrive at the final prototype, shown in **Figure 4**.

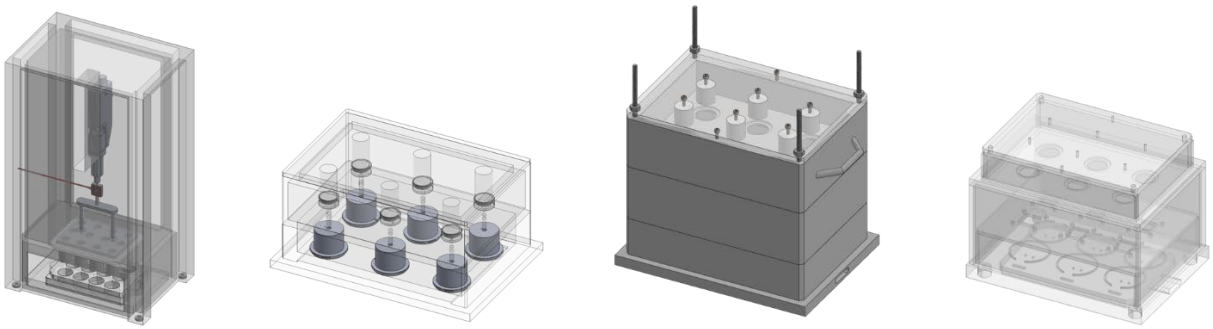

Figure 3. A brief overview of the design evolution from ME 351 to ME 352.

Design Decisions and Team Organization

Much work previous semester, as reflected in **Appendix E**, went toward translating client need – via calculation, prototyping, and modeling – into design specifications, listed in **Appendix A**. With a method of actuation selected (voice coil actuation / VCA), however, alongside compressive interface material selection (polytetrafluoroethylene / PTFE), more physical work related to the overall fabrication of the device began.

Work, similar to the fall semester, was divided to optimize a parallel workflow: Griffin and Sydney worked to refine and build the final housing, while Jeffery and Emilio worked to refine and develop the circuitry to better meet client needs.

Housing Team: Bioreactor Housing and Actuation

Overall, fabrication of the bioreactor, as mentioned, was subdivided into two teams: housing and actuation. The housing team, as implied, worked to create the overall structure through which the VCA force output – managed by the electronics team – could be translated into uniaxial compressive stress within a cartilage explant culture. **Figure 4**, along with illustrating the successful completion of one portion of the design criteria (i.e., 'fits within the Henak Lab incubator'), depicts the final evolution of the efforts of that work. This prototype can be thought of as consisting of four separate modules, with ¼" laser-cut paneling used as connecting walls (detailed engineering drawings and a bill of materials can be found in **Appendix B** and **Appendix C**): the base, alignment module, sample tray, and compressive interface. Over the course of the semester, each saw significant time investment to ensure module-specific client needs were met.

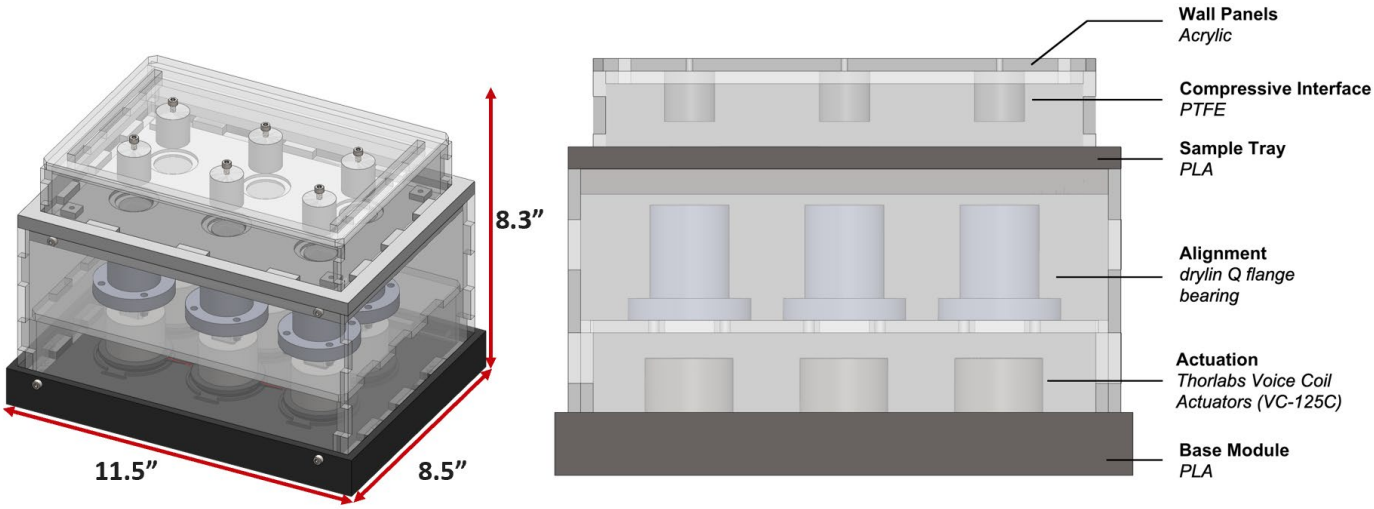

Figure 4. Dimensioned schematic of the final prototype, with an informal bill of materials (BOM).

Base

The first module, the base module (**Figure 5**), essentially serves as an anchor: it fastens both the rest of the bioreactor and the VCA in place. Printed with PLA and fastened to the acrylic side paneling via M4 fasteners – chosen to balance overall footprint with risk of shearing – the base also possesses (M4) through-holes aligning with those present in the VCA, allowing securing of the VCA to the base. Further, two pass-throughs for the wiring were implemented, allowing for the wiring to be accessed outside the bioreactor (i.e., therefore allowing the VCA to be controlled via circuitry kept outside the bioreactor).

Figure 5. Trimetric view of the sample base, with one VCA included for reference.

Alignment and Sample Housing

The alignment module, as the name suggests, serves to align the output of the VCA with a sample dish held within the sample tray and, obviously, the compressive pillar by which the desired +uniaxial compressive stress is applied. **Figure 6**A depicts the plunger system by which actuation between the VCA and sample dish is coupled, as well as the side profile of the fully assembled alignment system. Here, 3D-printed (BioMed Clear V1) mate components are press-fit into a 90 [mm] length aluminum profile sourced from the manufacturer of the square bearing (drylinQ), with an M6 bolt securing the VCA to the plunger. The bearing itself is secured via M4 bolts to a ¼“ laser-cut acrylic shelf suspended via acrylic cut-outs, with the weight of the bearing sufficient to prevent any vertical translation arising from the friction (**Appendix D** details expected lifetime friction for the bearing) between the aluminum profile and bearing when in operation.

In turn, **Figure 6**B depicts the mentioned sample tray, also printed with PLA and possessing M4 through-hole locations for further fastening of the bioreactor. These fastener locations, via the attached acrylic paneling, fasten 1) the base to the tray and 2) the tray to the compressive interface, thereby sequentially fixing each level of the bioreactor to the base. The sample tray, as noted, was designed (and, qualitatively, successfully tested) for compatibility with a standard 35 [mm] sample dish.

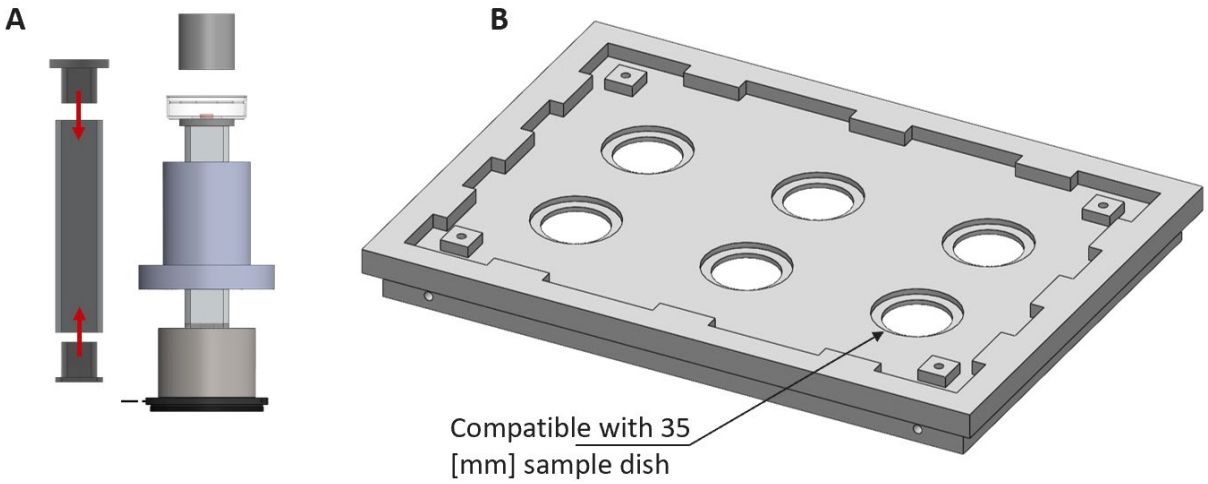

Figure 6. Overview of the alignment system and sample tray. A) Side view of the square bearing, used to prevent shearing arising from parasitic rotation of the VCA during use. B) Trimetric view of the sample tray.

Compressive Lid

The final, module-wise, component of the bioreactor is the compressive lid (**Figure 7**) – a ¼“ laser-cut acrylic panel, with the requisite through-holes to 1) fasten the PTFE pillars to impart compression and 2) secure the lid to the paneling. To ensure the acrylic lid was capable of withstanding forces beyond the upper range of expected use, SolidWorks finite element analysis (FEA) was applied. Fastener locations were fixed with the appropriate (fastener) boundary conditions, and a 10 [N] surface load was applied to the lower vertical face of each PTFE pillar. Both engineering strain (**Figure 8**) and failure criteria were analyzed to determine risk of

warping/deflection and failure, respectively. Regarding the former, FEA shows minimal risk of warping, as observed in **Figure 8**, with the bulk of the acrylic deflecting (vertically) less than 5 [µm]. On the latter, the Maximum Normal Stress criterion was applied, given its suitability for brittle materials such as acrylic, providing a factor of safety of 3.3. Overall, then, via FEA, ¼" acrylic was verified as a viable material for the compressive lid.

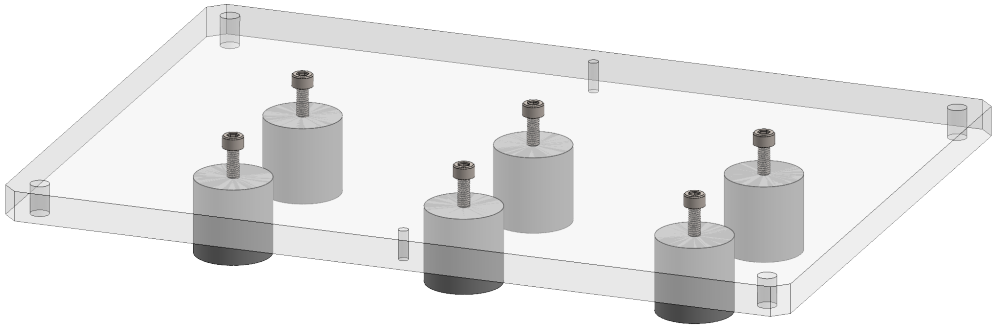

Figure 7. Trimetric view of the final compressive lid, with attached PTFE pillars.

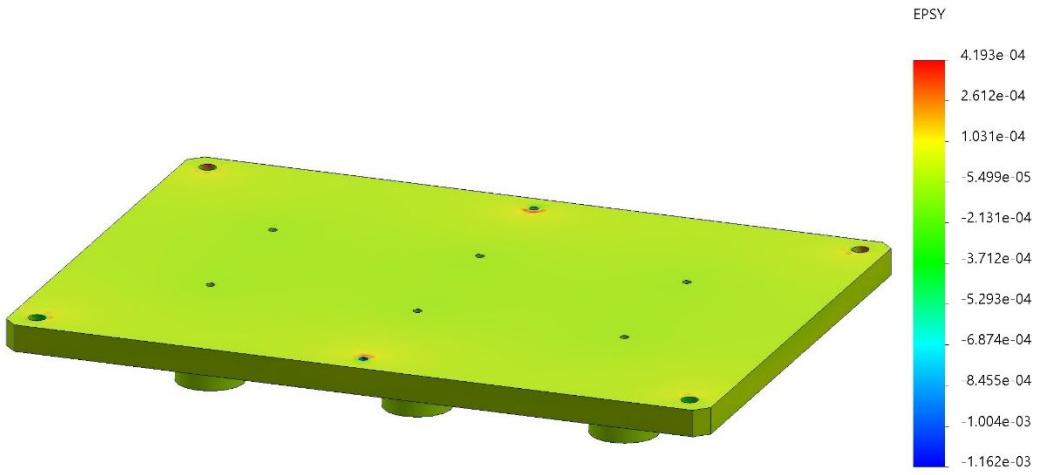

Figure 8. SolidWorks FEA of engineering strain arising from maximum expected (60 N) loading. Only the strain in the (vertical) y-axis, due to potential concerns of vertical warping and consequent heterogeneity in compressive profile, was considered.

Circuitry Team: Actuation Control

To power the voice coil actuator, a circuit must be designed to alternate voltage and provide a high enough current. To output the previously calculated 5.5N of force (Hookean approximation, **Appendix E**), the voice coil needs an input of around 6.6V at 0.7A. To generate this input, the team employed and compared different circuits to operate the voice coil.

Triangle Wave Generator PCB

The first circuit design is a triangle wave generator soldered onto a PCB as seen in **Figure 9** below. The PCB was designed and fabricated by Professor Mark Allie from the electrical engineering department. The main feature of this design is the built-in triangle wave generator with a voltage regulator. The PCB can be easily powered by plugging in a wall adaptor to have a triangle wave output. The voltage can change between 9V-12V by changing the jumper clip on the pin. Each pin represents 9V, 10V, 11V, and 12V respectively. The voltage can then be fine-tuned using the amplitude potentiometer. Similarly, the output frequency can be effectively changed using the potentiometer on the board itself.

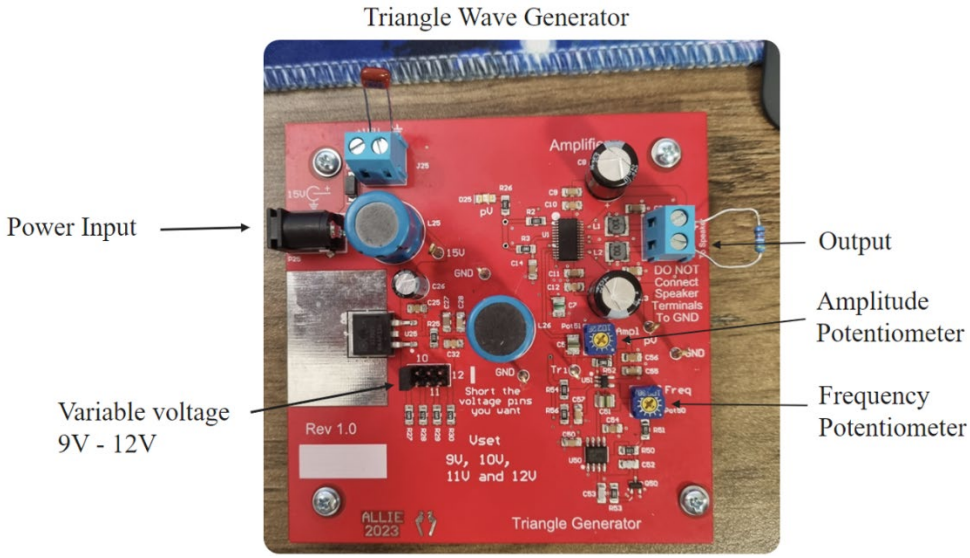

Figure 9. Triangle wave generator soldered onto a PCB with annotations.

From the experimental results shown in **Figure 10** below, it was found that the output of this triangle wave generator is capable of outputting a triangle-like wave. It looked more like an RC discharging-charging wave as opposed to a triangle wave. The recorded frequency was 2.59Hz and could not https://bmedesign.engr.wisc.edu/course/schedule go any lower. This was because the components used to design had a safety feature built into them. Thus, it disallows any frequency lower than 2.59Hz to run else it will automatically shut down. The effective duty cycle was also around 50.28%, which is quite close to what was expected – a 50% duty cycle. The recorded voltage when the 9V clip was equipped with the amplitude potentiometer turned to the minimum was a peak-to-peak voltage of 4.38V. This brings the attention to the resolution of the voltage will be more defined as the voltage can only be fine-tuned using potentiometer. To change the potentiometer itself, a screwdriver will be needed to turn the knob. This makes fine tuning the voltage a challenge.

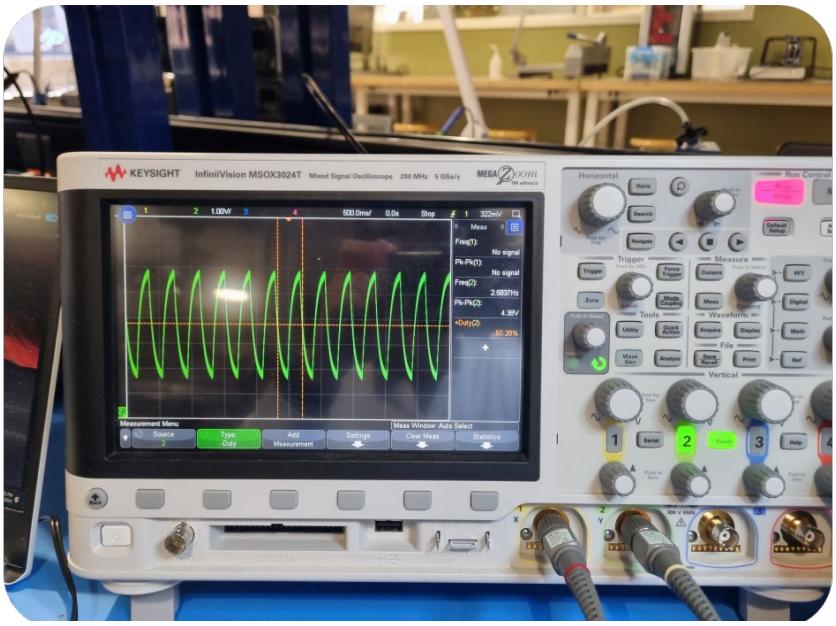

Figure 10. Output from PCB on an oscilloscope.

H-Bridge

The second design utilized an L298n H-bridge motor controller. A simple circuit design was made to operate the H-bridge. This can be seen in **Figure 11** below. The circuit comprised of two components - a microcontroller and the H-bridge, and can connect up to two voice coils each. The H-bridge is to switch the voltage's polarity at a set frequency. This frequency is programmed entirely by the microcontroller. In **Figure 11** below, the H-bridge is controlled by an Arduino Uno microcontroller. The code used to operate the H-bridge can be found in **Appendix H**.

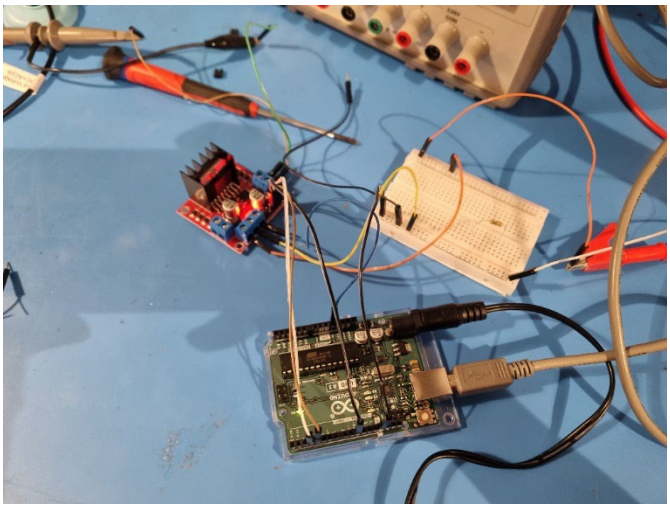

Figure 11. Circuit layout of the H-bridge with Arduino.

After some experimentation, some data were collected on the oscilloscope as seen in **Figure 12** below. It was found that the H-bridge is capable of outputting 1Hz with a peak-to-peak voltage of 620mV. Given how the output voltage is not desired, an additional component might need to be added to the circuit to reach 6V. Overall, the H-bridge might not be the most

suitable circuitry to pursue as the H-bridge drives the voice coil actuator in both directions. Since the voice coil actuator is placed vertically, there isn't a need for it to be pulled back rapidly. Thus, a circuit that is designed to drive the voice coil actuator in one direction would be sufficient.

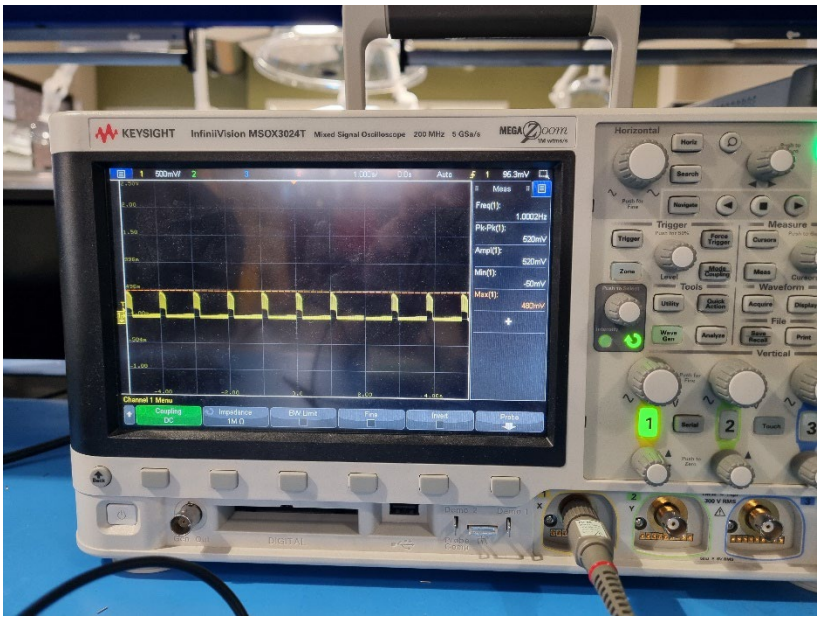

Figure 12. Output from H-bridge observed on the oscilloscope.

Transistor

To tackle the bi-directional nature of the H-bridge, a different circuit was designed with the idea of having a single directional output. By using a similar concept of the H-bridge, a transistor circuit was designed. The circuit is composed of an NMOS transistor, a diode, 1kΩ resistor, 1MΩ resistor, a power supply, and a microcontroller. An NMOS transistor is advantageous over a PMOS transistor as it has a better switching speed – the rate at which it turns on and off, and a lower on-resistance. This would ensure a smoother change, lower energy dissipation, and less heating due to a lower resistance. A diode is used to protect the voice coil actuator from a backflow in current, and the power supply supplies the voltage and current directly to the voice coil. The microcontroller is used to control the frequency at which the NMOS switches on and off, enabling the voice coil actuator to operate.

The LTSpice schematic and breadboard circuit can be seen in **Figure 13** below. From the breadboard circuit, the Arduino is the representation of the NI DAQ, the battery is the representation of the power supply, and the voice coil actuator is represented by the vibration motor. The ports of the Arduino are exactly the same as with the NI DAQ, in which port A0 on the Arduino would reflect onto port AO0 on the NI DAQ. Screen captures of the front panel and block diagram of the LabVIEW VI are provided in **Appendix I**.

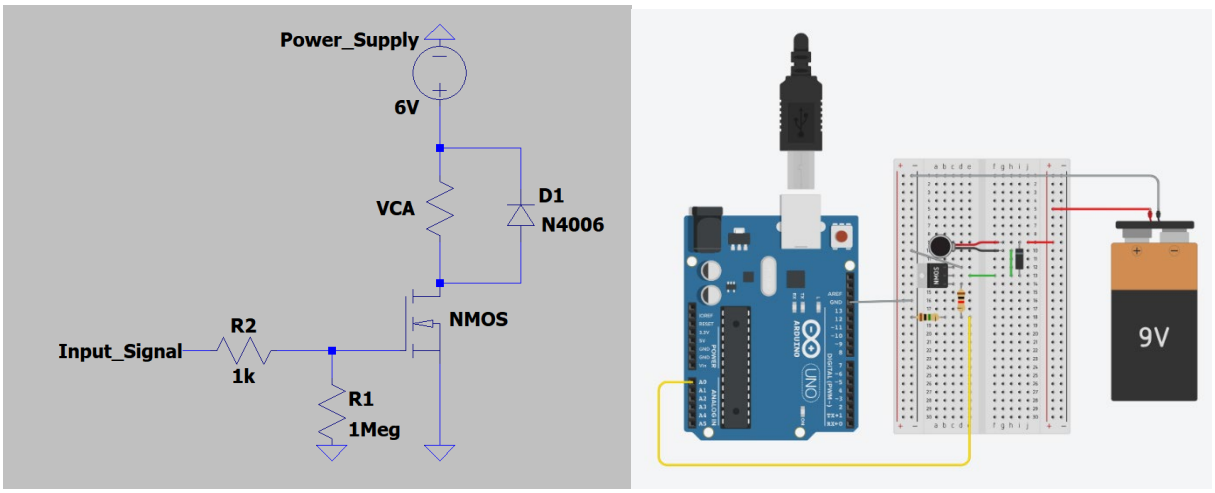

Figure 13. LTSpice Schematic of circuit (left) and breadboard circuit (right).

After going through some testing, a triangle wave was observed by averaging the wave profile. The output was recorded to be at 1Hz with a peak-to-peak voltage of 2.89V when the power supply input was 3V. This can be seen below in **Figure 14**.

Figure 14. Output from NMOS circuit observed on the oscilloscope.

Design Matrix

To compare each of these circuits, a design matrix was used. This can be seen below in **Table** . Each of these circuits were ranked based on functionality, ease of use, space and compactness, and cost from 1 to 5, with 5 being the highest. Functionality refers to how versatile the circuit would be in terms of varying input signal such as using a sinusoidal wave. Ease of use refers to how easy it is to change variables such as voltage and frequency of the circuit. This also includes how easy it is to set up the circuit. Space refers to how compact the circuit can be when accommodating 6 voice coils actuators. Lastly, price refers to how much the entire circuit would cost. Each of the aspects used were ranked based on the importance relative to the project specification.

Table 1. Design Matrix comparing each circuit designs.

Criterion (Rating)	PCB	H-Bridge	Transistor
Functionality (15)	1 (3)	5 (15)	5 (15)
Ease of Use (10)	2 (4)	3 (6)	4 (8)
Space (10)	2 (4)	3 (6)	5 (10)
Price (5)	5 (5)	1 (1)	1 (1)
Total (40)	**16**	**30**	**34**

In terms of functionality, the H-bridge and the transistor circuit were ranked the highest as they were operated by a microcontroller. Thus, the input signal can be changed easily by changing the program code. Since the PCB has a triangle wave generator soldered onto it, it would be difficult to change the output signal to a signal other than a triangle wave. Thus, it was ranked the lowest.

For ease of use, the transistor was ranked the highest as it was the code was the easiest to change. The H-bridge's code interface requires more change as the code is longer. The PCB was ranked the lowest as it uses an amplitude potentiometer to change the effective voltage and frequency. Since it was a screw type of potentiometer, the resolution would be lowest amongst the three circuits, making it the most difficult to use when it comes to precision.

For space, the PCB was ranked the lowest as each PCB can only be used to power one voice coil actuator. Thus, having 6 of them would take would be space demanding and requires 6 adaptor ports. The transistor circuit scored the highest as it is the most compact amongst the three circuits. If considering a breadboard, approximately 3 circuits can be placed onto one. All 6 circuits can be powered by a single power supply provided the power supply can provide the necessary current and voltage. Yet, the transistor circuit can be even more compact if it were to be soldered onto a board, making it the least space consuming.

As for cost, both the H-bridge and transistor circuits utilize minimal electrical components. The H-bridge and transistor circuit components cost less than $20 to control all 6 voice coil actuators while the PCB would cost around $50. Thus, both the H-bridge and the transistor circuit were ranked the lowest.

Overall, the transistor circuit was ranked the highest with a score of 34/40. Hence, the team decided to move forward with the transistor circuit to drive the voice coil actuator.

Results and Discussion

Housing: Prototyping and Fabrication

In order to turn the housing design after its many iterations into a version most suited to fit client specifications, two generations of housing were fabricated. The first of which was constructed to help elucidate any potential issues with bringing the until-then only 3D CAD model to life. The thought was to discover any modifications that could be made streamline client use and bioreactor functionality that were only readily apparent in a physical object. With this prototype constructed and debuted at the preliminary prototype presentation, fabrication of a final bioreactor housing to be presented to the client could begin.

Preliminary Housing Prototype

Before fabrication of the preliminary prototype, the CAD was first changed to reflect all the actual measurements of the materials to be used. Most crucially to this, the bioreactor's side walls were all sized to be ¼" thick and include tongue-and-groove connections. This was to ensure that when fabricated, everything would fit together and there would be no surprises regarding incompatible dimensions. With this ensured, the prototype was constructed out of the aforementioned ¼" laser-cut clear acrylic side panels and was fit with a 3D-printed PLA base and sample tray. It was fastened together using hot glue where the tongue-and-groove connections weren't strong enough on their own. Below in **Figure 15** is the 24"x36" SolidWorks drawing sent to the Makerspace laser cutter to create the panels.

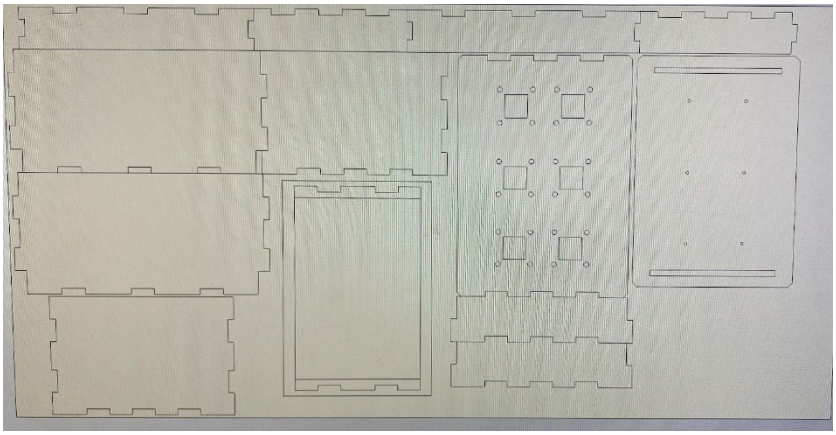

Figure 15: SolidWorks drawing of the 24"x36" acrylic sheet to be laser cut. Tongues and grooves were fit together as much as possible to optimize for space.

Once cut, the acrylic panels could be assembled into something that vaguely resembled the bioreactor. A quick sanity check at the Makerspace was done by fitting all the panels together to ensure that a) they were the appropriate size and b) they all fit together snugly. This can be seen in **Figure 16** below.

Figure 16. Quick assembly of the bioreactor's acrylic panels to demonstrate their compatibility immediately after cutting.

With the acrylic panels cut, the base and sample tray could be fitted with tongue-and-groove connections that matched with the acrylic's and sent to the 3D printer. 15% infill tough PLA was selected as the print material due to its low cost. Both prints were successful on the first attempt. With all materials ready, the bioreactor prototype could be assembled in full. This can be seen in **Figure 17** below.

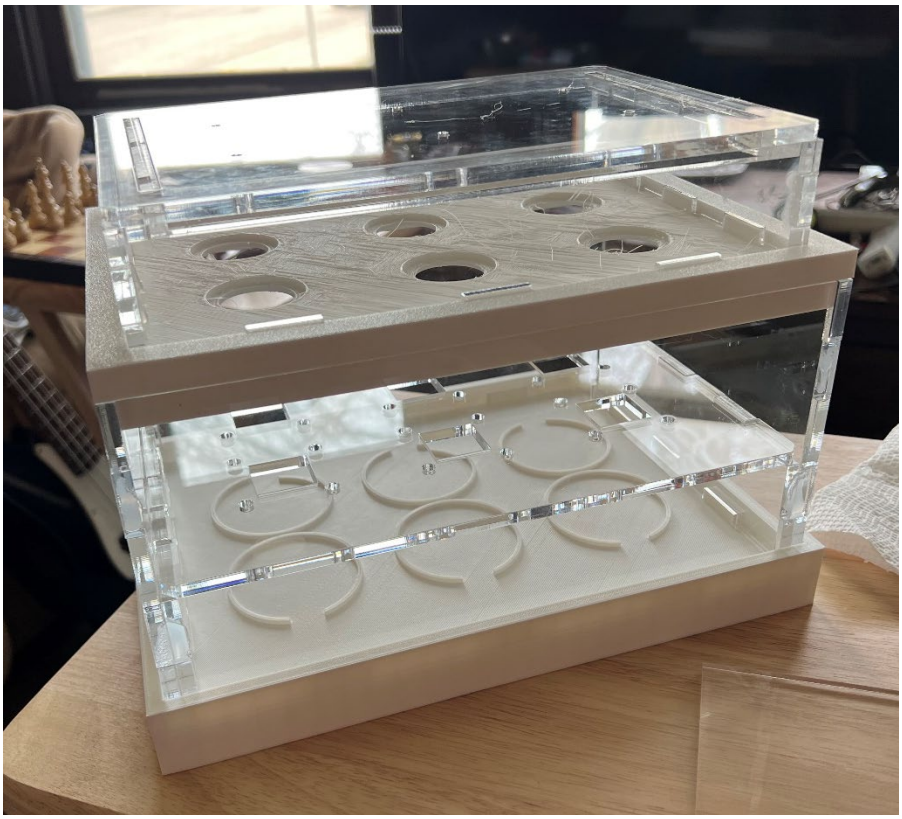

Figure 17. Fully assembled bioreactor prototype attached with hot glue in vulnerable spots.

This prototype helped accomplish several things related to helping optimize the final design. The first of which was that after modification of the base CAD to be the correct shape and size, the through-holes for fasteners and wires were filled in. This was an easy fix and was changed in the final prototype. The second large accomplishment of the prototype was to help the team think about how the client could access the samples in a way that still permitted secure closure while the bioreactor was in operation. To do this, reinforced through-holes were added to the sample tray at each of the corners. These were then fitted with a 3D-printed post that had a threaded rod in the top where a compatible wingnut could be detached and reattached when the samples needed to be accessed, as seen in **Figure 18**. The posts were secured to the sample tray using M4 bolts and to the side panels using epoxy.

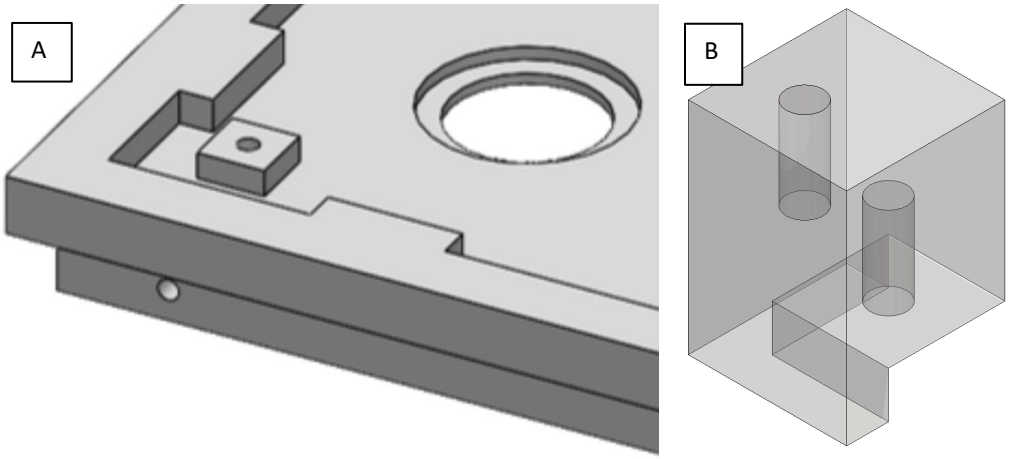

Figure 18: (a) Trimetric CAD view of the sample tray's reinforced through-hole for post attachment. (b) CAD of posts to be fitted to the sample tray.

Other mechanisms for fitting the lid to the sample tray were devised and evaluated before the team selected this design. The first of which involved the use of eight total bolts fit with wingnut heads that could be used to tighten and loosen the sample tray's connection to the lid and base assemblies. Once removed, the sample tray could be lifted off the base and the acrylic lid panels could be lifted off of the sample tray. The second mechanism relied on removable dowels in the same locations as the wingnuts would be, except they were instead tightened together with the force of a Cable Clamp. A Cable Clamp essentially works like an easily attachable and detachable zip-tie. It would tighten the dowels together, once on each corner, by sliding the teeth into the insert. **Figure 19**(a-c) shows sketches of these designs on the CAD.

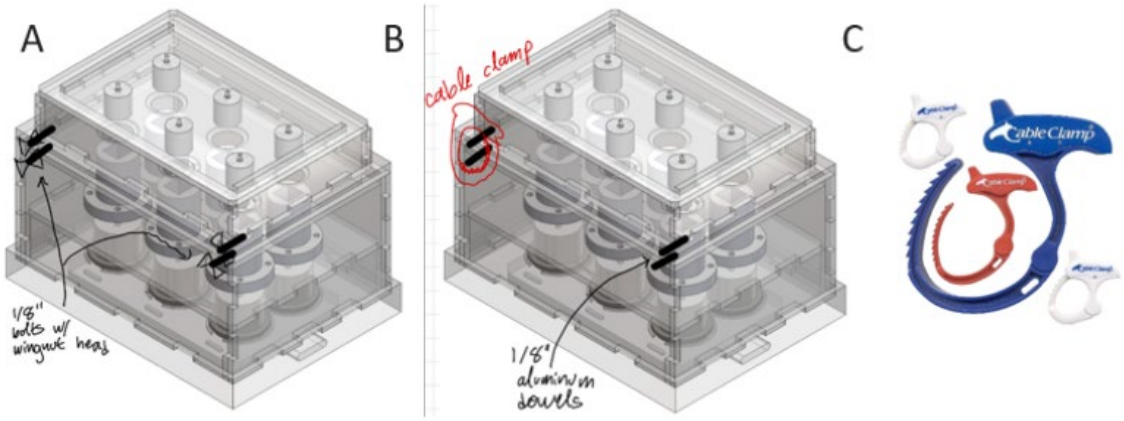

Figure 19. (a) Wingnut attachment on the sides of the sample tray permitting complete separation of the sample tray from acrylic panels. (b) Removable dowels in the sample tray that could tighten or loosen the connection of the lid to the sample tray with use of a Cable Clamp. (c) Image of a cable clamp for reference.

The first design was sub-optimal because eight wingnuts attached to the sample tray is not a very efficient way to access the cartilage samples within the bioreactor. The second design alleviated this slightly by only requiring insertion of eight dowels and tightening them with ergonomic Cable Clamps. However, there was some slight concern over the bending moments that the Cable Clamps would introduce when tightened. Pulling down on the upper dowels and up on the lower dowels would introduce new strains into the sample tray that would have the potential to warp it or potentially even cause it to break. Rather than performing a formal solid-modeling analysis of this potential problem, the team devised another strategy that would a) alleviate these bending moments and b) involve less work to attach and detach the compressive lid. This mechanism was incorporated into the final design.

Final Housing Prototype

Informed greatly by the initial housing prototype, a final housing prototype was constructed that at its current stage can be used in experimentation by the Henak Lab, seen in **Figure 20**. This design has both through-holes for circuitry and fasteners as well as an easily detachable compressive lid.

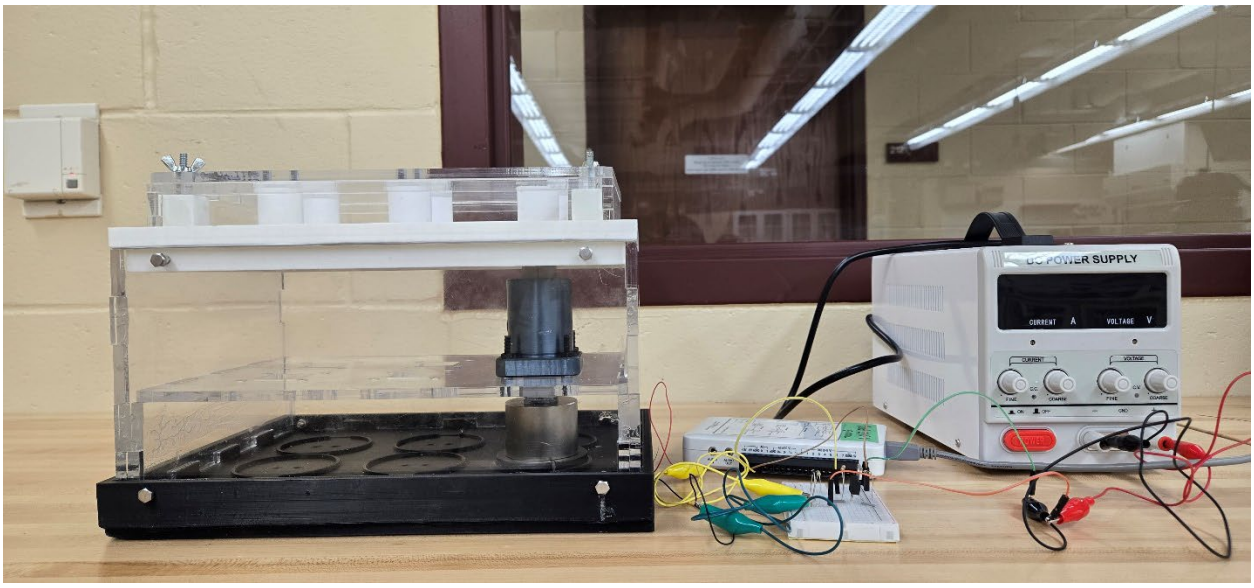

Figure 20. Final housing prototype.

Most of the same acrylic panels were used in the preliminary and final prototypes. The only new panels were the lid's walls, which needed to be made shorter to be in the stroke range of the VCA so that the sample could contact the PTFE. The bioreactor was fixed together using a variety of fasteners, including M4 bolts and nuts for panels to dish and tray, M6 machine screws and washers for PTFE pillars, and 8/32” threaded rods and wingnuts for the lid posts. The acrylic panels were fixed together using epoxy purchased at the Makerspace. Once fully assembled, it was ensured to be structurally sound.

In terms of difficulties in the fabrication process, the biggest and most frequently recurring was the need to drill additional holes in the acrylic. It was both cheaper and less time-

consuming for the team to use a drill press and create the holes where they would fit with those in the base and sample tray as it was printed rather than to measure their placement, add them to the CAD, and recut the entire panel. It was challenging to get the exact hole placement with the first pass, so several drill passes had to be made in some cases. In the case of the lid, the holes were sized up much beyond 8/32" to facilitate easy matchup with the threaded rods. A concern with drilling was that the acrylic, due to its brittleness, would shatter and the piece would need to be remade completely. Thankfully, this was mitigated successfully by drilling smaller pilot holes before sizing up to the necessary size.

The only significant error in the fabrication process was that the base was epoxied to the base's acrylic panels. This was not intentional and was the result of several long hours of fabrication and a small brain slip. This means that the bolts affixing the base's panels to the base are technically obsolete, though they do provide additional structural support. The reason this is an issue is that now it would be much more difficult to replace the base in the bioreactor with something machined out of aluminum, which can be autoclaved. Though PLA can be sanitized with ethanol, this is more of a pain for the Henak lab to do rather than to use an autoclave. Even with this error, the bioreactor's function is unimpacted.

Circuitry: Load Cell Testing

Objectives

To validate the performance of our voice coil actuator against the design specifications, we performed force profile tests using the Henak lab load cell. The primary objectives of the testing were to ensure that the force output remains permissibly constant over longer durations of operation (i.e., 15-30 minutes), ensure the actuator applies to desired amount of force (i.e., roughly 5.5-6 N), and to check for any deviations such as overshoot.

Testing Setup and Procedure

The load cell testing setup included securing the actuator on the base of load cell and interfacing the actuator, a small rubber sample, and force sensor. Our tests included three tests which operated the actuator at frequencies of 0.5 Hz, 1 Hz, and 2 Hz. The DC power supply, which controls force output, was set to output a fixed voltage which generated 5.5 N of force for all tests. Running each test at the desired frequency, the load cell recorded the force profile overtime at durations from 15 to 30 minutes.

Results & Discussion on Testing

Force profiles were successfully obtained at the three tested frequencies along with 15 second snapshots, depicted in **Figure 21** through **Figure 26** below. From the results of the load cell testing, the force profile most closely resembles a square wave, although it is more triangle-like at higher frequencies. By a visual, qualitative judgment, the force profile is indeed relatively constant at the target force setpoint (i.e., 5.5 N) over the duration of testing, as desired.

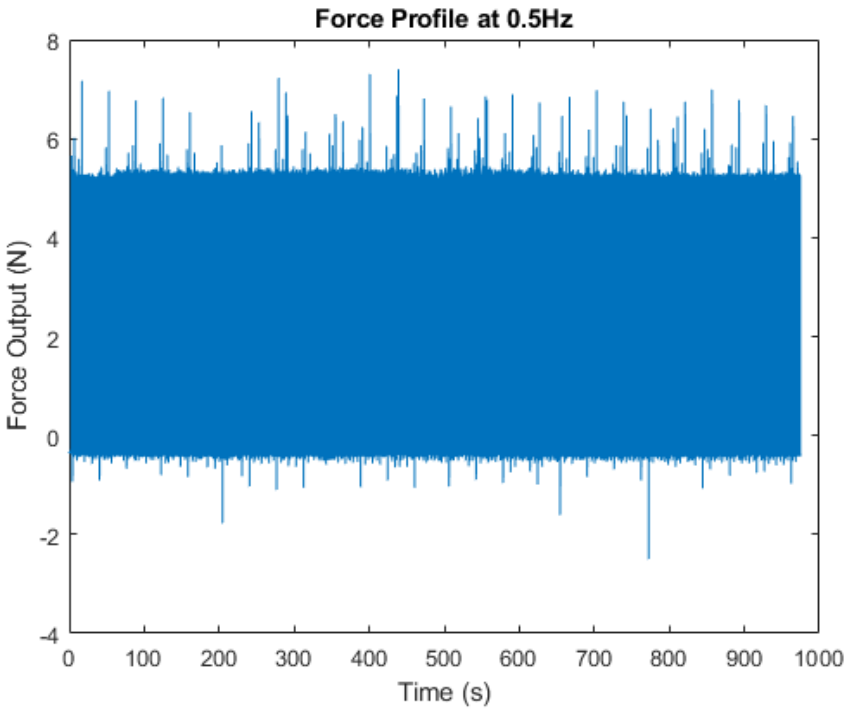

Figure 21: The force profile obtained at 0.5 Hz.

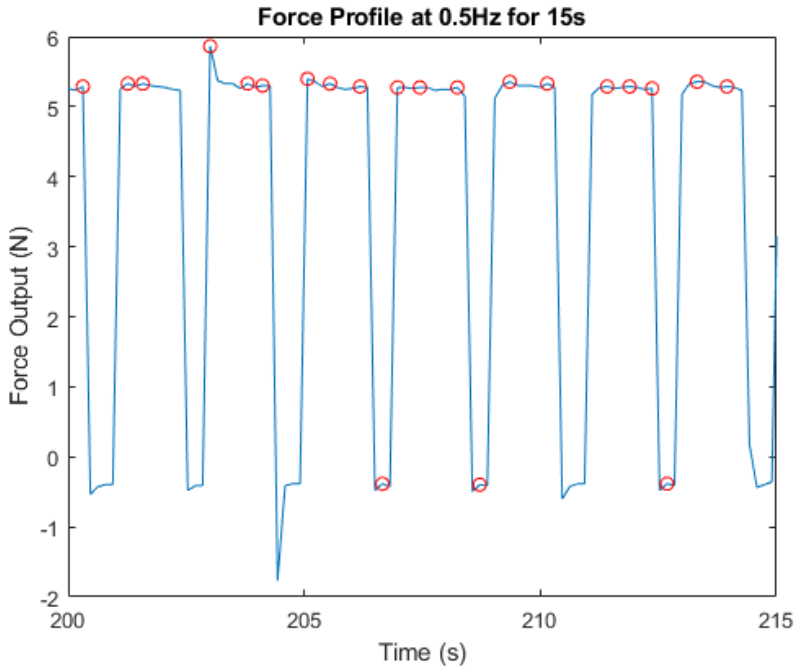

***Figure 22*:** A 15 second snapshot of the force profile obtained at 0.5 Hz.

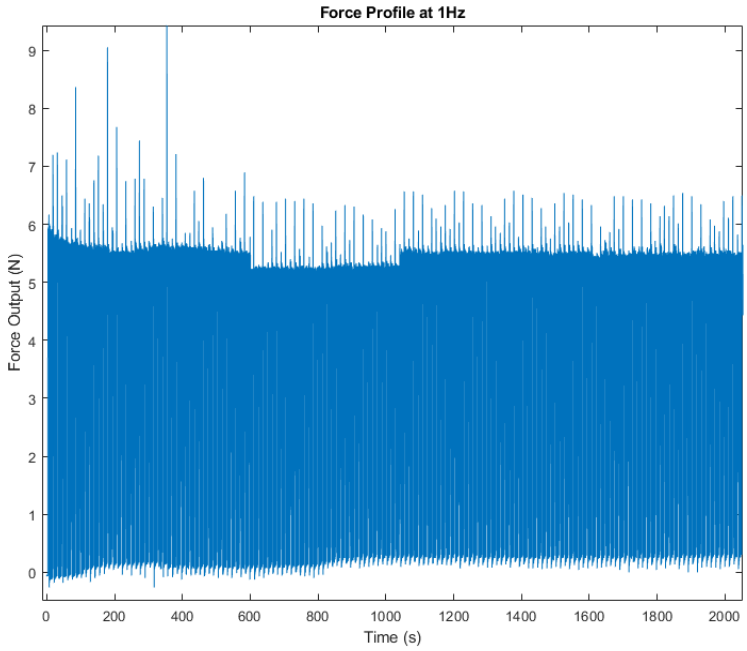

Figure 23: The force profile obtained at 1 Hz.

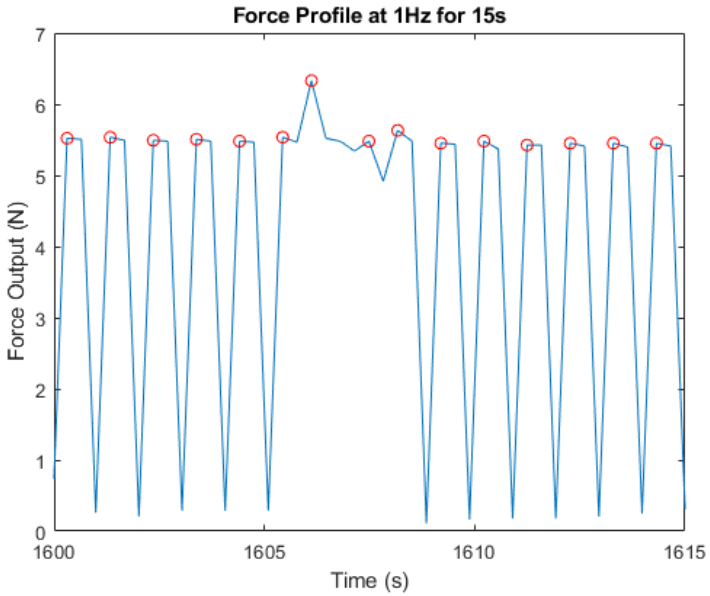

Figure 24: A 15 second snapshot of the force profile at 1 Hz.

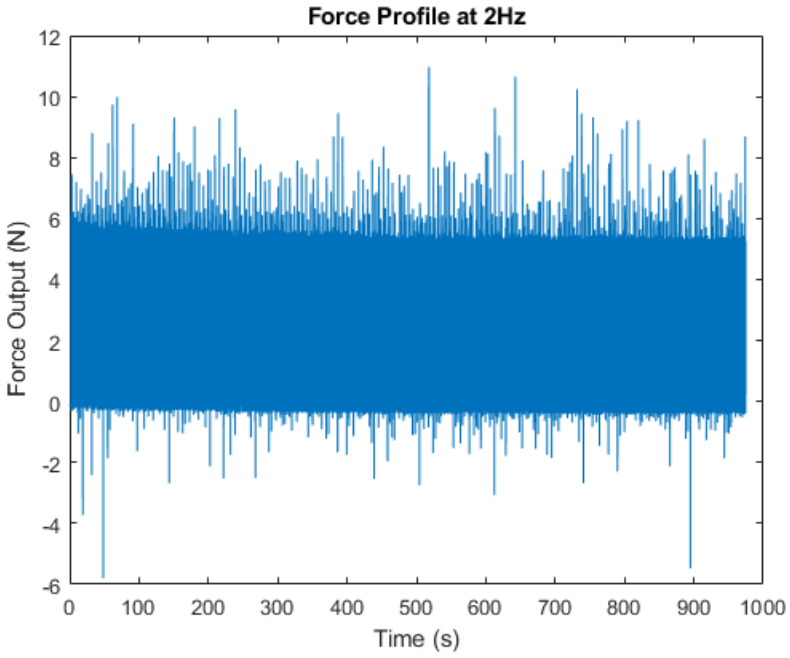

Figure 25: The force profile obtained at 2 Hz.

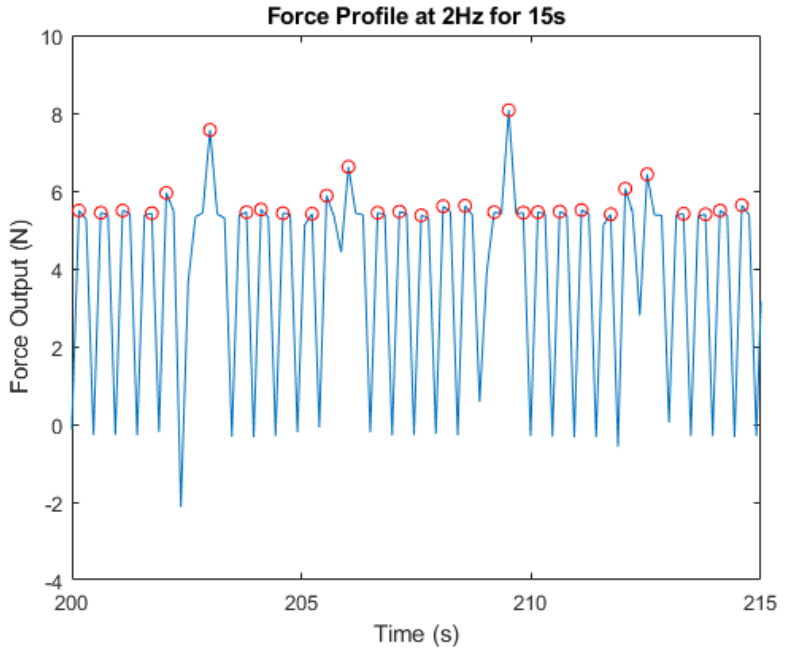

Figure 26: A 15 second snapshot of the force profile obtained at 2 Hz.

We also conducted an initial consistency test, where we slowly increased the power supply voltage slowly from zero. The test, whose force profile is depicted below in **Figure 27**, shows relative consistency around the target force value of 5.5 N as well. We also created a FFT from the consistency test to obtain the frequency response of the actuator at 1 Hz, shown below in **Figure 28**.

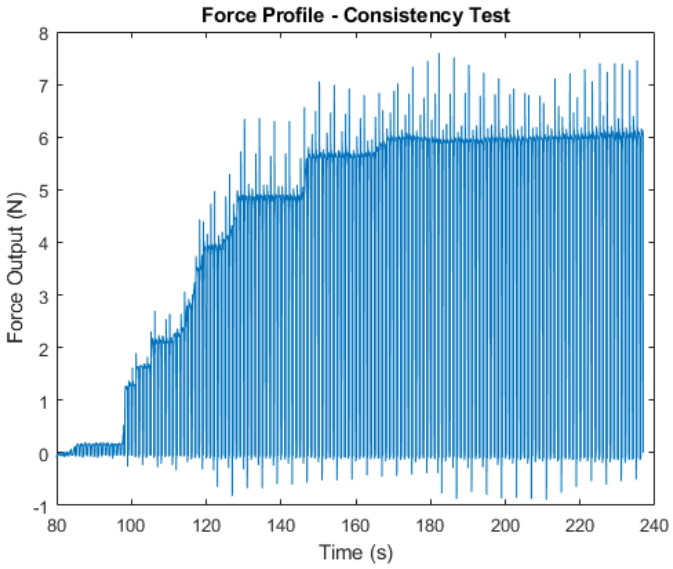

Figure 27: The force profile obtained from the initial consistency test, performed at 1 Hz.

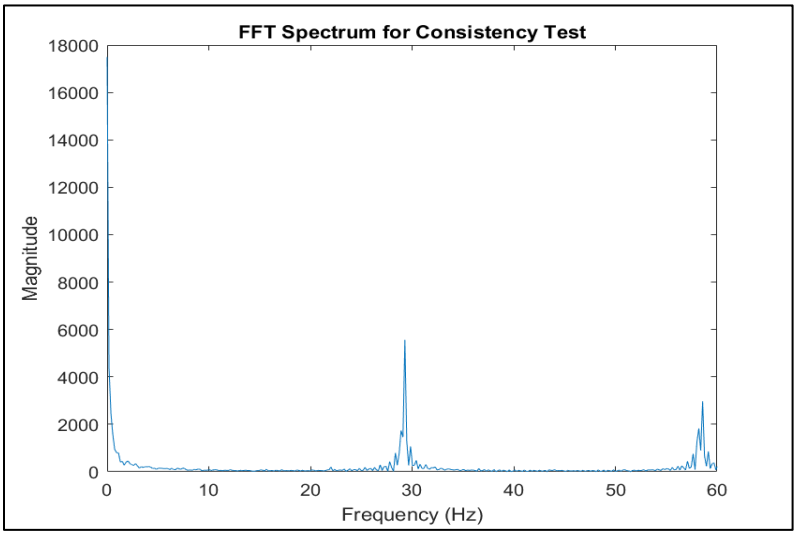

Figure 28: FFT frequency response obtained from the initial consistency test.

Overshoot

Force profiles revealed the presence of overshoot exceeding the desired force setpoint. While voice coil actuators such as the Thorlabs VC125C/M are known to have great precision over their force output, we observed overshoot whose cause is not fully understood. We quantified the overshoot for all tests as a percentage, summarizing their values in a plot, depicted below in **Figure 29** through **Figure 31**. Overshoot was computed according to **Equation 1** below. Note that the load cell outputs negative force readings in compression, which is the case for our testing. Overshoot was only calculated when compressive force exceeded 5.5 N, and a value of zero was returned when the force reading was less than 5.5 N.

Equation 1: The equation used to compute the percent overshoot from 5.5 N of compression when testing the actuator under the load cell. The calculation is a simple percentage difference.

$$\%\ Overshoot = \frac{F_{applied} - (-5.5\ N)}{-5.5\ N} \times 100\% \quad (1)$$

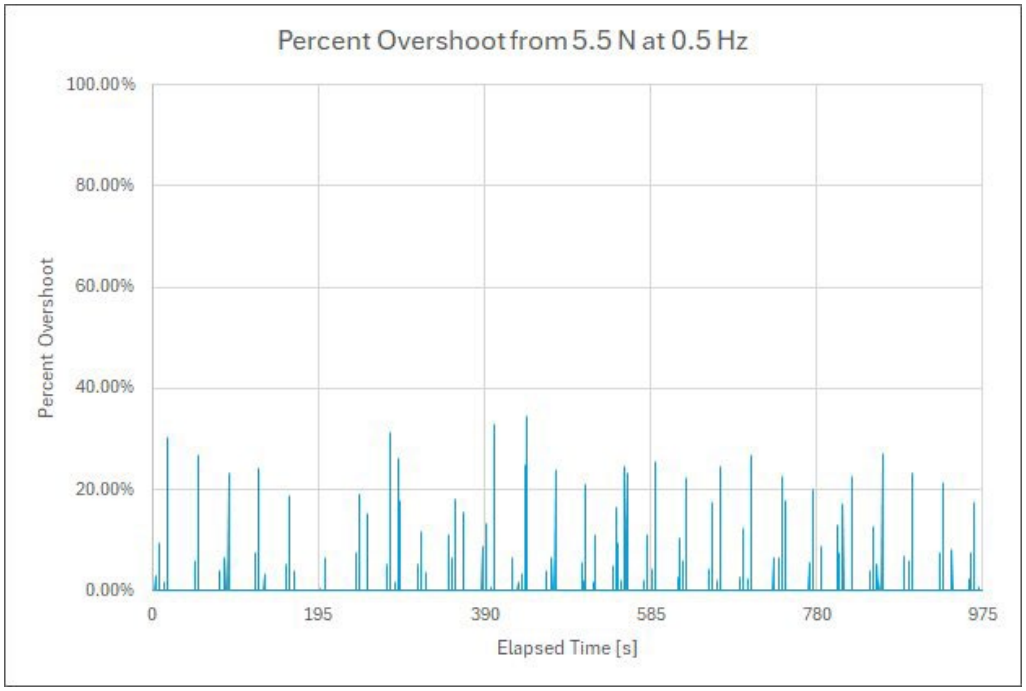

Figure 29: Percent overshoot from 5.5 at 0.5 Hz.

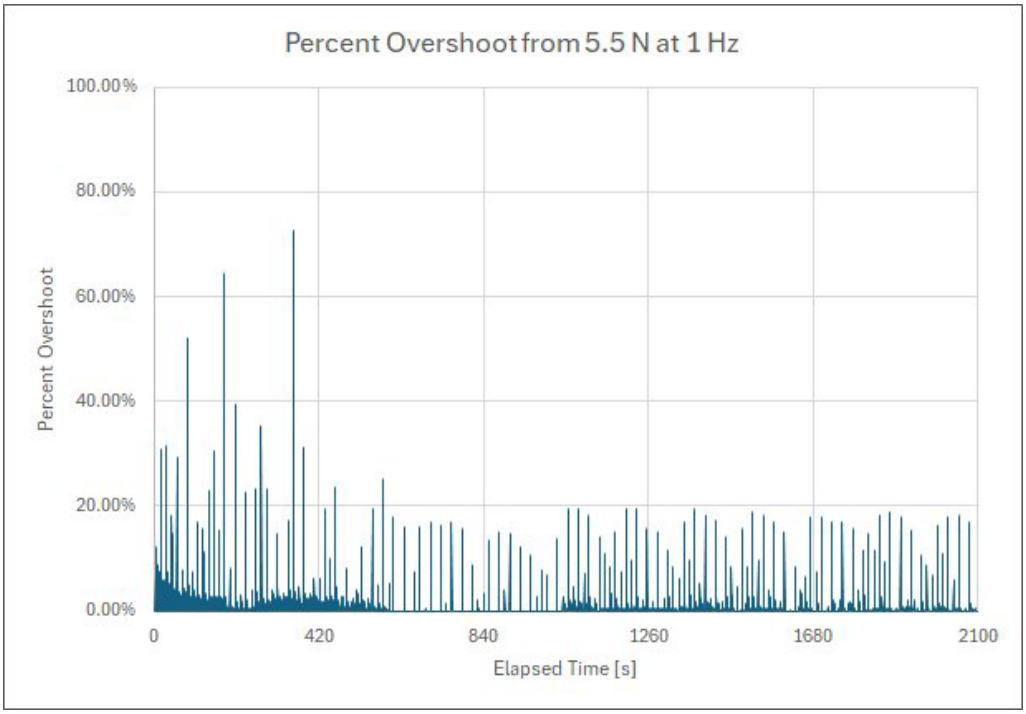

Figure 30: Percent overshoot from 5.5 N at 1 Hz.

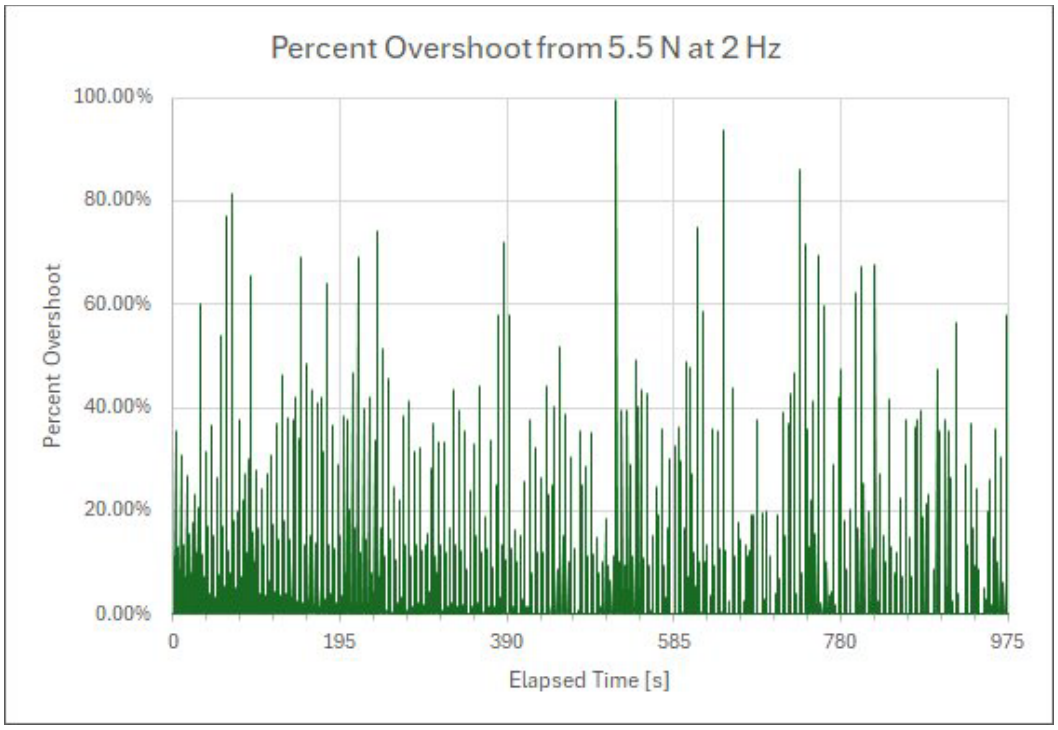

Figure 31: Percent overshoot from 5.5 N at 2 Hz.

By visual, qualitative judgment, the plots above suggest that overshoot is generally more prevalent at higher frequencies. The averages, medians, standard deviations, maximums corresponding to percent overshoot were also computed, tabulated below in **Table 2**. These statistics were computed only for nonzero values of overshoot. The 0.5 Hz test experienced the largest percent overshoot from 5.5 N but also experienced the smallest maximum percent overshoot. The 2 Hz test, however, experienced the largest maximum percent overshoot. The cause of overshoot is not fully understood. It's possible that overshoot can be attributed to the magnetic base of the load cell. Because the VCA was not elevated from the base of the load cell, it's possible the VCA magnet interacted with the magnetic base during testing, contributing to overshoot as the VCA would need to overcome the magnetic force from the base. We did not calculate undershoot, which is a behavior that may be of interest to determine into the future. Undershoot did not occur frequently compared to overshoot, however.

Table 2: Summary of overshoot statistics for testing at 0.5 Hz, 1 Hz, and 2 Hz.

Overshoot	0.5 Hz	1 Hz	2 Hz
Mean	11.44%	2.12%	9.84%
Median	7.62%	0.64%	3.38%
Standard Deviation	9.14%	4.52%	14.65%
Maximum	34.58%	72.78%	99.51%

Conclusion and Future Work

After one academic year of progress, the team is pleased to report that a bioreactor has been designed and built that has the ability to test a single cartilage sample in an experimental setting. Furthermore, the bioreactor's housing can test six samples if more components are ordered and integrated. The design specifications have all been met to varying degrees of success, but there are still improvements to be made that could elevate the utility of the bioreactor. Both specification validation and future work will now be discussed.

Specification Validation

The design specifications for the bioreactor were broadly grouped into three categories: physiological force output, incubator compatibility, and budget fidelity.

In terms of the physiological force output, the primary goal was to create a force output that induced ~20% engineering strain in cartilage samples, which equated to ~6N of force when analyzing the mechanical properties and dimensions of cartilage (this calculation is available in Appendix E). This was validated using load cell testing of the actuator, which yielded an average of between 5-6N during the majority of testing. These results were discussed more in-depth in the load cell testing section, in which plots verifying this can be seen. It was further required that this deflection was force-controlled, meaning that due to creep attributed to the poroelastic behavior of cartilage, the sample's height would eventually decrease, and the sample would no longer be in contact with the compressive interface were simple deflection control be used. This was ensured by the selection of a VCA, which creates force control by modulation of voltage and current. This force must be applied in a cyclic pattern to induce the physiological loading that the Henak lab wishes to study. As such, a triangular loading profile was created by the circuit. And finally, the cartilage samples must contact an interface that is as low-friction and biocompatible as possible to ensure sample integrity. This was ensured by the selection of PTFE as the compressive interface material. The engineering analysis of PTFE selection can be found in Appendix E. Overall, the team can truthfully report that all specifications in the physiological force output category are successfully achieved.

Regarding compatibility with the incubator, it was to be ensured that the bioreactor can fit inside, withstand the high temperatures and humidities, and be sanitized in accordance with Henak lab procedures. The dimensions of the bioreactor are 11.5 x 8.5 x 8.3 in^3, which comfortably fit in an incubator with inner dimensions of 20 x 21 x 25 in^3. All materials selected (acrylic, PLA, stainless steel fasteners) can withstand the 37C physiological temperature and high humidity. The largest concern regarding temperature was the VCA, the magnet on which can become more easily damaged at higher temperatures. According to the specs of the selected VCA, significant magnet damage begins to occur at temperatures over 110C. This is well below the temperature that the VCA will operate, so it is not a concern. In terms of sanitation, all components of the housing can be wiped down with ethanol. The PTFE pillars can be autoclaved, which is important as they are in direct contact with the biological specimens. Therefore, all specifications relating to housing are achieved.

The team was given $5000 with which to design and build this bioreactor with an additional $200 stipend from a Plexus grant specifically for fabrication use in university

facilities. The team is happy to report that only $730.22 of this was spent on the design as it exists currently. Should the Henak lab choose to scale up the bioreactor to test more samples at a time, this will require purchasing another five VCAs, bearings, and shafts. The associated estimated cost of this is $3777.72, which is still below the $5200 budget. Should the Henak lab choose to order machined aluminum versions of the base and sample tray from the TeamLab, the estimate provided for this during a design consultation was ~$1200 for labor and materials. This still brings the entire bioreactor's cost to $4977.72. This is within budget, which satisfies the budget fidelity specification. This means that all specifications set at the beginning of the semester have been achieved.

Future Work

With careful planning and analysis, the team successfully met all bioreactor specifications. However, there are certainly still steps that can be taken to improve the bioreactor so that it is easier to use. These can broadly be grouped into the same categories as the design specifications.

To ensure that the force output from the VCA is indeed physiological, the entire bioreactor should be tested in a load cell with the bearing integrated. Former force testing was done with the actuator alone, which does not ensure that the force output will be the same with the rest of the design integrated. To prove this, the team recommends that the Henak lab perform an experiment using the bioreactor as-is to see if it is performing as-desired. This could then be followed up with load cell testing of the bioreactor to examine the actual forces that were applied to the sample. It could be found out during this process that 20% engineering strain is not replicating the physiological situation that the Henak lab wishes to model, and this change can be implemented with knowledge of how the circuit actually runs. If the Henak lab wishes, the triangle profile could be switched to a sinusoidal profile to run more smoothly and physiologically. This would also reduce and impulses that the jab of the triangle profile creates.

To improve the housing and its integration into the incubator, some or all the materials can be switched out with machined aluminum, or steel for a higher price. This would mean that the entire housing with the VCAs, bearings, and circuitry disconnected could be autoclaved. This would improve workflow for the Henak lab and ensure a higher degree of sanitation between experiments.

The last recommended next step for the bioreactor would be to scale it up to incorporate six samples. As mentioned in the specification validation section, this additional cost would not exceed the budget even after machining the entire bioreactor out of aluminum. This would allow more replicates to be tested when characterizing the long-term metabolic impacts of cyclic loading on cartilage, which would produce higher-fidelity data.

Summary

To help the Henak lab study the disease progression of osteoarthritis, a bioreactor is required to characterize the long-term metabolic impacts of cyclic loading on cartilage. This is filling an important gap in the literature, where this progression is less understood over longer timescales. The bioreactor was designed to house six cartilage samples, which are cyclically loaded by force-controlled VCAs that create a physiological triangular loading profile. The bioreactor is housed in an incubator, which all materials used in the bioreactor's construction can withstand.

This bioreactor will help inform the future of osteoarthritis research and provide key insight into how to best treat this high-impact disease.

Appendix A: Design Specifications

Table A-1: Client needs (i.e., customer requirements) and engineering design specifications for the force-controlled cartilage bioreactor.

Client Needs					
Client Need Statement					
To investigate the relation between cartilage redox balance and disease state, the Henak Lab requires a method of applying physiologically relevant mechanical stimuli (which is known to influence said redox state) to articular cartilage samples over the long-term; to meet this need, Dr. Henak has requested the fabrication of an incubator-housed device capable of replicating in vivo compressive stimuli profiles over the desired timescales.					
List of client needs (in their words)					
Low-to-no friction on contacting pillar surface					
Linear actuation applying ~20% strain to 6mm x 2mm (diameter x height) cartilage samples					
Constant force, not necessarily constant strain, applied across all samples					
Device must be capable of providing a variety of force profiles					
Incubator-compatible					
Specification description	**Target**	**Unit**	**Test method**	**Rank**	**Met**
Category 1: Device Function					
Device to apply & control linear actuation with controlled force capable of actuating compression mechanism	>6	N	Validate manufacturer specifications with testing	Must	MET
Induces 20% strain in (idealized) cartilage samples via uniaxial compressive stress	0.2	mm/mm	Use in-device load cell to determine deformation	Must	MET (via theoretical calculation and relation of force output)
Sufficient device actuation to allow for removal of sample dish	10	mm	attempt removal of sample dish	Must	MET
Low-friction compression/interface with cartilage sample	0.1	-- (coefficient of friction)	Manufacturer Specifications [19], [20]	Must	MET

Category 2: Incubator and environment					
Fit within incubator	(20 x 21 x 25)	inch	place fully fabricated box into incubator / measure	Must	MET
Able to withstand laboratory-grade sanitation procedures	---	---	Review of individual electronic technical specifications prior to use	Must	MET (ethanol)
Electronic components of actuator withstand incubator's simulated in-vivo environment	---	---	Review of individual electronic technical specifications prior to use	Must	MET
Cords of electronic components may be wired to external power sources	---	---	review of cord diameter and quantity	Must	MET
Category 3: Additional Functions					
Modular compressive pillar attachment (i.e., to allow for 6, 12, 24, etc. well plates to be used)	---	---	N/A	Nice-to-have	MET
Modular compressive pillars that are different shapes (e.g., indentors)	---	---	validate that the actuator applies the same force to the samples	Nice-to-have	NOT MET
Re-feeding mechanism (i.e., to change sample media automatically within incubator)	---	---	N/A	Nice-to-have	NOT MET

Appendix B: Bill of Materials (BOM)

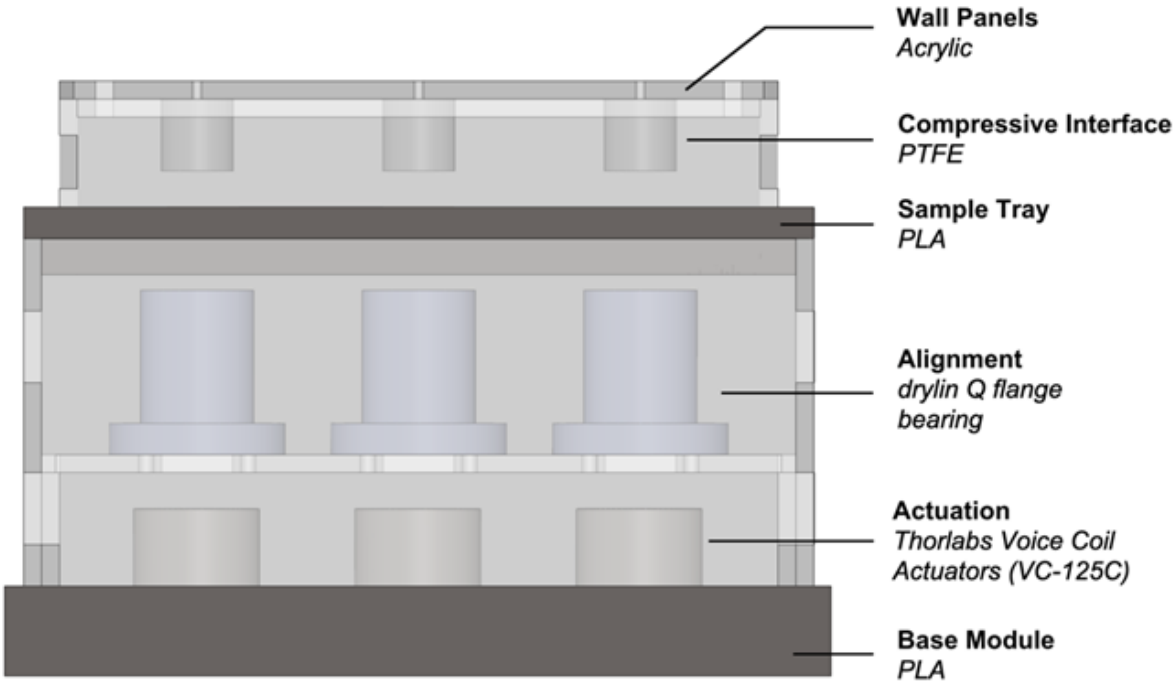

Base Module & Sample Tray: PLA Makerspace Ultimaker S5

Acrylic Paneling and Lid: 0.25” acrylic (Makerspace)

Actuator: Purchased from ThorLabs – VC125C/M

Alignment:

- Bearing: drylinQ Square Flange; Round Bearing
- Profile: drylinQ Square Profile (Cut to length; 90 [mm])
- Mating Components: BioMed Clear V1

Compressive Interface:

- PTFE: 1” diameter rods; McMaster Carr

Electrical Components:

- Breadboard
- Diode N4006
- NMOS Transistor IRLZ44N
- Resistors 1kΩ, 1MΩ
- DC Power Supply DCP3010D
- NI DAQ USB-6001 or Arduino Uno

M4 & compatible wingnuts/nuts used for all fastening, apart from the lid-to-tray fastener (M5).

Appendix C: Final Engineering Drawings

All necessary CAD files are uploaded into a shared Box folder. Relevant, brief engineering drawings of the base, tray, and plunger system are shown here. All drawings are in millimeters & degrees.

Base:

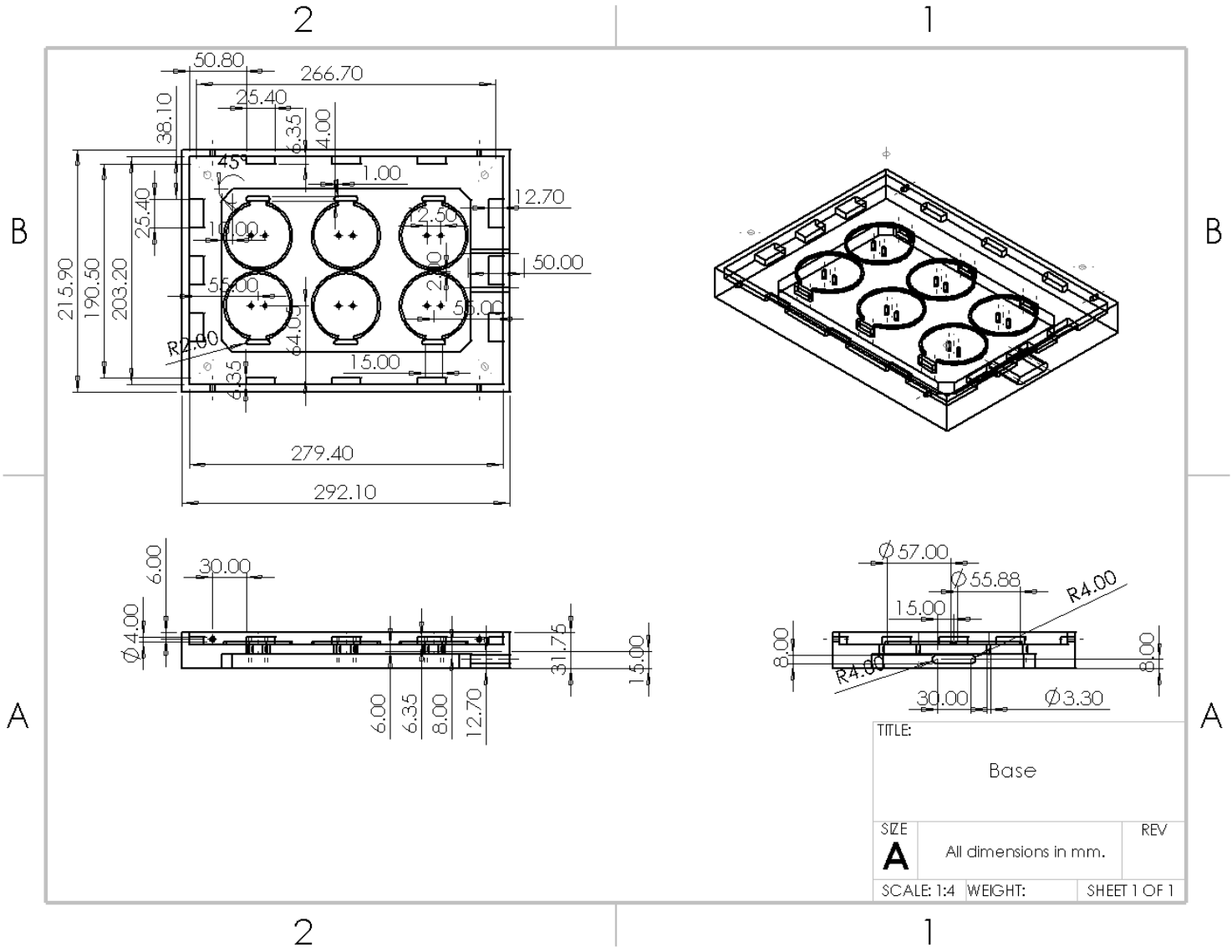

Tray:

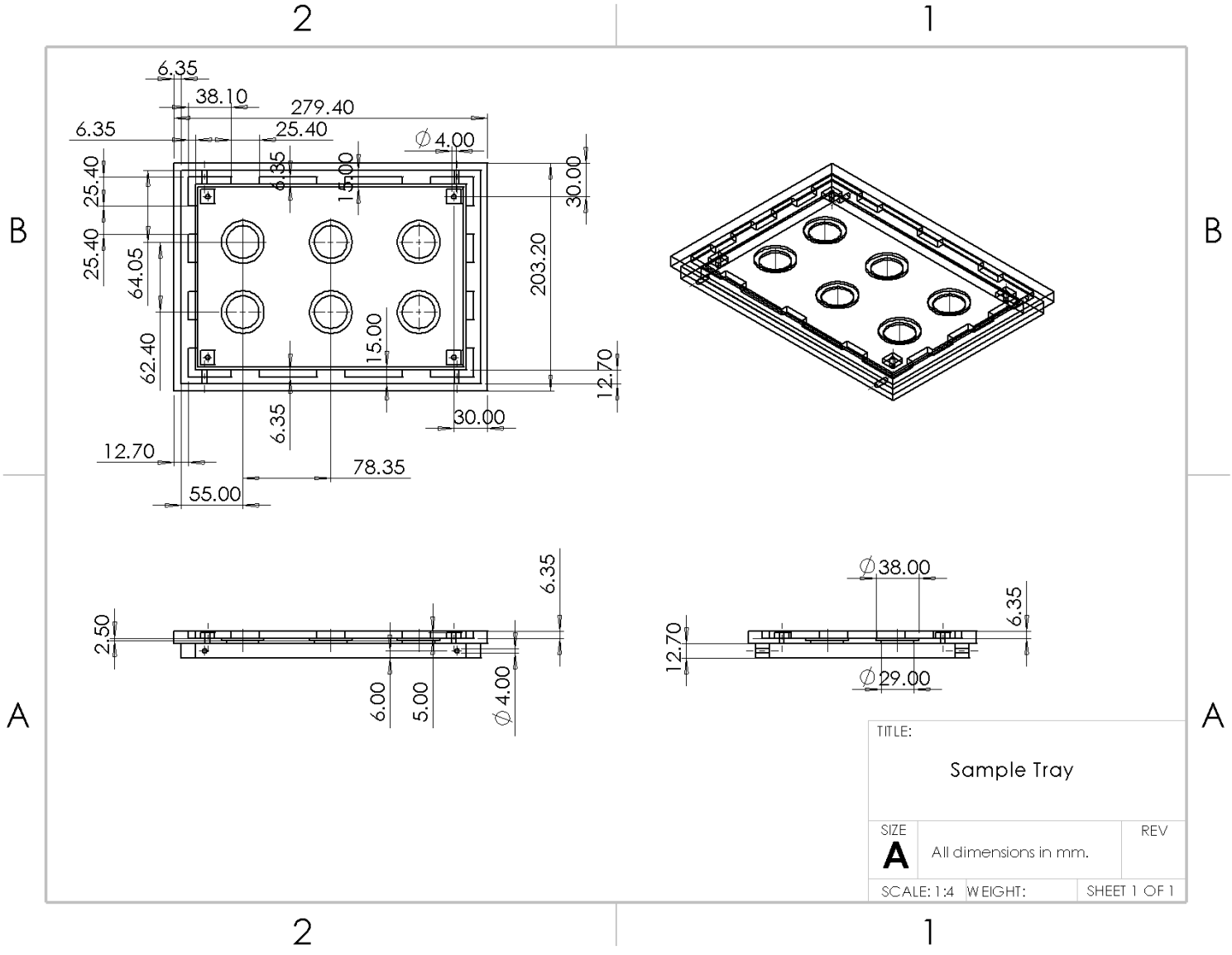
2
1
B
A
6.35
38.10
279.40
6.35
25.40
∅4.00
25.40
6.35
15.00
30.00
25.40
64.05
203.20
62.40
15.00
12.70
6.35
30.00
12.70
78.35
55.00
6.35
2.50
6.00
5.00
∅4.00
∅38.00
6.35
12.70
∅29.00
TITLE:
Sample Tray
SIZE
A
All dimensions in mm.
REV
SCALE: 1:4
WEIGHT:
SHEET 1 OF 1

Plunger System:

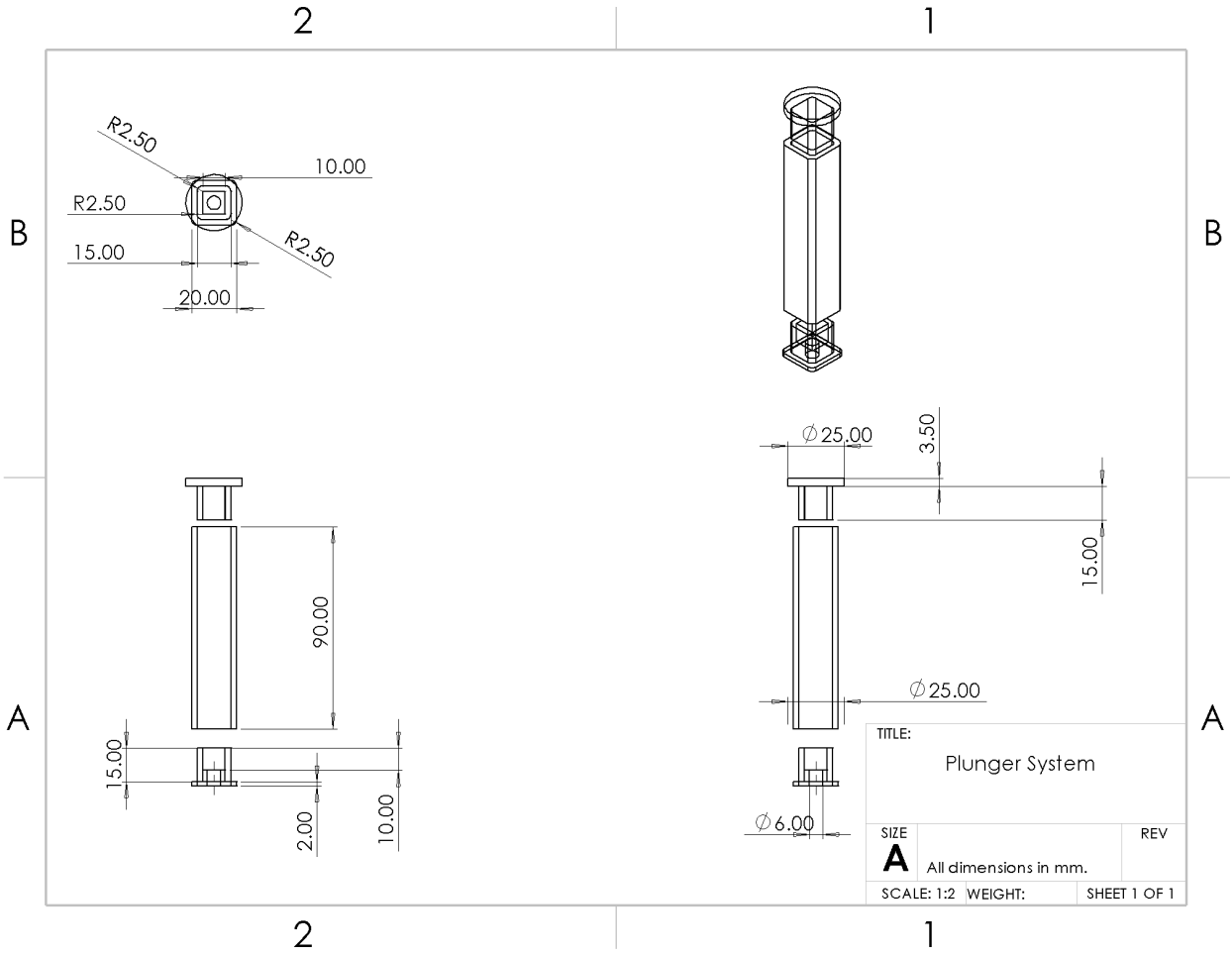

Appendix D: Bearing Design Matrix & Friction Analysis

Products Under Consideration

1. Drylin Flange Bearing, Round Flange
    a. A little large, 20mm internal diameter square (no smaller options)
    b. Lead time: by feb 15th (16th at this point probably)
    c. Could configure it with something like this square post and put that directly in the actuator? We could also fabricate something like this
2. Misumi Flanged Ball Bearing
    d. This is a really good ball bearing with a flange that should be good dimensions for us but we need a shaft!
    e. (specs)
3. Misumi Complete Ball Spline
    f. Basically perfect but pricey
    g. Some specs

	Friction (40)	Shafts (15)	Re-orderability (10)	Cost for all six (35)	Totals
Drylin Square Flange	(⅕) mu=0.19 with stainless steel and ideal smooth finish	(⅖) Square and almost 1in^2, very big	(⅗) Depends on where shaft comes from but bearing is a reorderable product	(⅘) $382.92 (+ shafts)	48
Misumi Flanged Ball Bearing	(5/5) mu=0.003-0.006 but for the square ones, same design ish so should be similar	(⅗) Cylinder with race, would need to machine or call to find part	(⅗) Depends on where shaft comes from but bearing is a reorderable product	(5/5) $100.20 (+ shafts)	90
Misumi Complete Ball Spline	(5/5) mu=0.003-0.006 but for the square ones, same design ish so should be similar	(⅘) Would need to be tapped or threaded, or could order it this way for more $$$	(5/5) Can order again from a Misumi no issue	(⅖) $1170.18	76

Friction Analysis

After the TeamLab consultation steered the team in the direction of using the Drylin Q flange bearing (essentially for cost/lower complexity reasons), I wanted to see whether or not use of this bearing would fulfill the design specifications. This involved assessing the friction force that would be produced between the walls and the shaft, and the lifetime of the product using wear resistance.

To assess friction, I first called igus to see if the CoFs on the website were static or dynamic (it did not say). They said that the values would be comparable between the two, so for estimation purposes, I used the provided values for low and high loads (I'm fairly certain this is a low-load application, but I wanted to visualize both). Using Ff = mu*N and a range of normal forces from 0-3N (hopefully much more than we would hope to experience) and multiplying by four for the number of walls that experience the friction, I produced this plot.

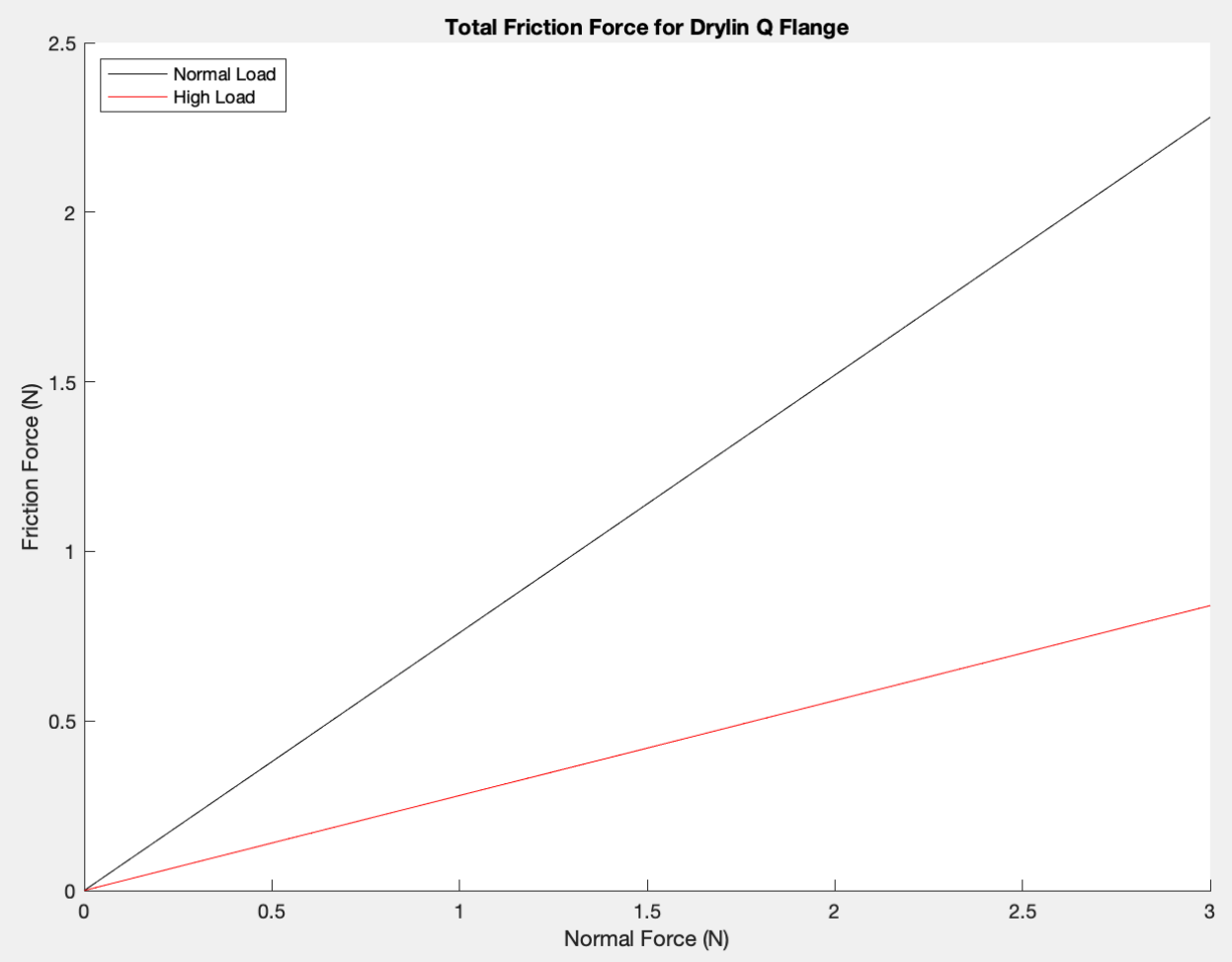

Figure 1: Plot describing the total friction force opposing actuator output force for the Drylin Q flange bearing over a range of normal forces.

Since the force output range for the VCA goes up to ~12N, this friction force is easily compensated for if the device is calibrated properly. However, the normal force fluctuates depending on the amount that the walls with low-friction gliding material are worn down. I wanted to assess how

fast this process happened to both see how often the device would need to be recalibrated and how long the bearings would last before the low-friction gliding material wore down enough to necessitate replacement.
I pulled wear coefficients from the Drylin website. These were given in um/km, which I interpreted as "the gliding material will wear down this many microns if 1 km of shaft slides across it." These wear coefficients were given for many shafts, the lowest two of which for our gliding material (iglide J) were hard-anodized aluminum and hard-chromed. Drylin sells a hard-anodized aluminum shaft compatible with this bearing for $101.19/m. I assumed that with each actuation, the shaft travels along the entire length of gliding material (which is a significant overestimate but provides us with a solid factor of safety). Using the wear coefficients, the distance of gliding material covered in one second (twice the length of how much is inside the bearing), and some basic math, I calculated how long the bioreactor could be in operation. This is shown below.

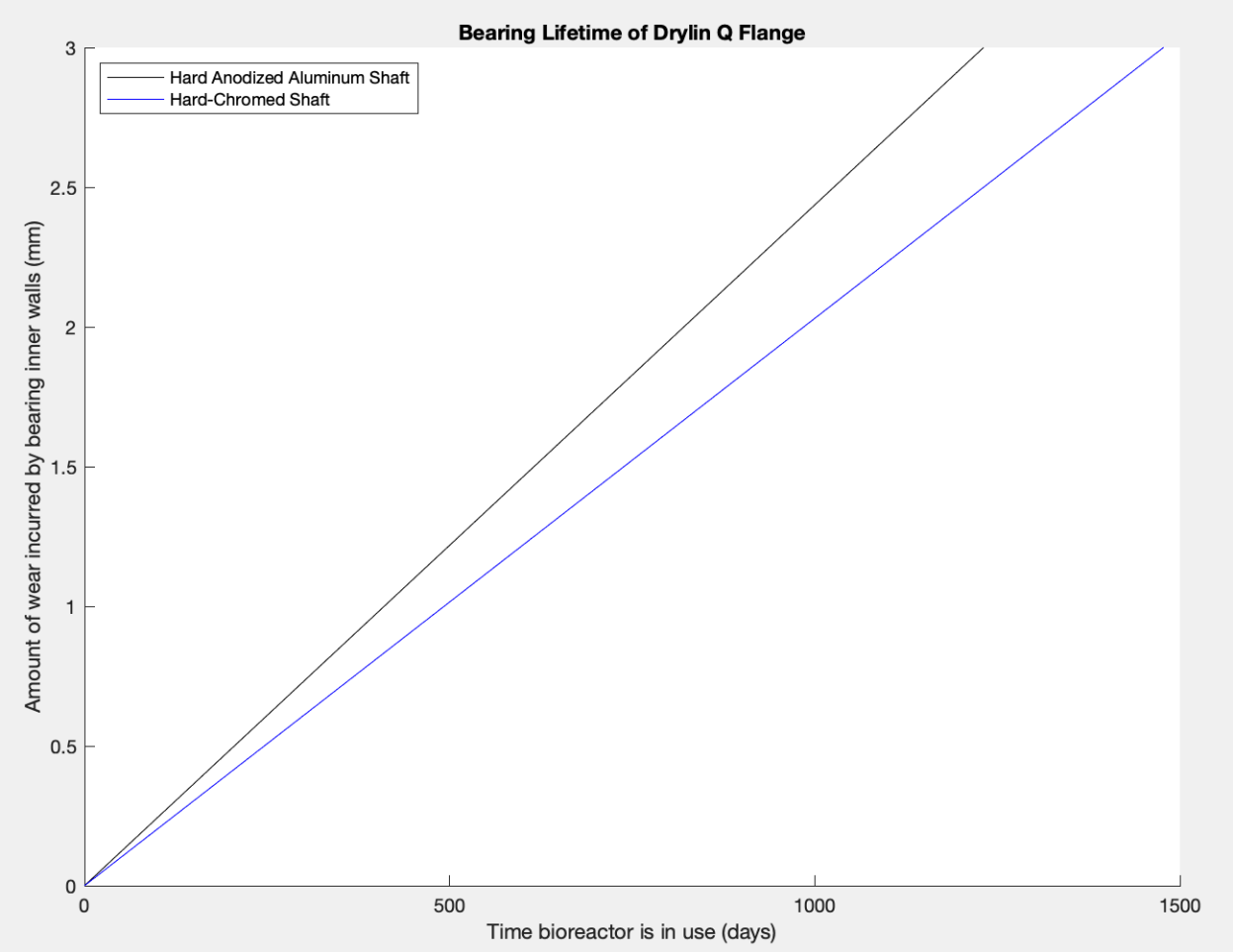

Figure 2: Plot describing how long the bioreactor is in continuous operation versus how much that operation wears down the walls made of gliding material.

What Figures 1 and 2 show is that the Drylin bearings have a much longer life than previously thought and seem to be a fitting bearing for the bioreactor. With this information, I hope that the team can be more confident moving forward with incorporating them into the design.

Appendix E: Prior Work (ME 351)

Determining Necessary Force

To fabricate a bioreactor that could induce the strain requested by the client, some calculations were performed to approximate the magnitude of the force required. This magnitude approximation will also inform what type of actuator is best suited for this purpose. This was done by relating two equations for stress: the 1st Piola-Kirchoff stress, or engineering stress, and the Young's Modulus equation. The 1st Piola-Kirchoff stress (π) equation relates force sustained after deformation to its reference area:

$$\pi = \frac{F_{applied}}{A_{reference}} \quad (1)$$

Where:
$F_{applied}$ = Force experienced by material after it has been fully deformed [N]
$A_{reference}$ = Cross-sectional area of sample before sustaining deformation [m^2]

Since the cartilage samples can be approximated as linear and elastic for the purpose of magnitude estimation, a rearrangement of the Young's Modulus equation can be used that solves for the stress experienced by the sample (σ):

$$\sigma = E\varepsilon \quad (2)$$

Where (with respect to the axis of loading):
E = Cartilage's approximate Young's Modulus [MPa]
ε = Engineering strain experienced by sample [$\frac{mm}{mm}$]

By setting the two stress terms π and σ equal, this creates an equation that can be used to solve for $F_{applied}$:

$$F_{applied} = E\varepsilon A \quad (3)$$

All variables in Equation 3 have been given as specifications. For cylindrical samples with a Young's Modulus of 1MPa, a 6mm diameter, and experiencing 20% strain:

$$F_{applied} = 5.7 \text{ N}$$

Therefore, the team will use 5.7N as an approximation of a reference range of forces desired by the Henak Lab to apply to the cartilage samples while in the bioreactor. It is sufficient to produce a ballpark number with some approximations because error in this value can be corrected for during the calibration of the actuator with the circuit.

Actuation Mechanism Selection

Several different mechanisms of actuation were considered to produce this force output. Based on the Lujan et. al. design, [8], the first mechanism considered was a voice coil actuator (VCA) system. To perform a thorough analysis of the available options, hydrostatic, pneumatic,

and closed-loop displacement control systems were also evaluated. Each of these mechanisms was researched and will be detailed in this section.

Voice Coil Actuators.
VCAs are an electric and force-controlled mechanism of force application. When current is fed through the wire coil in the base, the wire coil interacts with the magnet assembly it is coupled to and produces a Lorenz force that thrusts the magnet assembly away from the base. In this way, force output is directly proportional to current input:

$$F = B\,x\,I \tag{4}$$

Where: [10]
F = Force [N]
B = Magnetic Flux Density [T]
I = Current [A]

VCAs are very precise since there are fewer places to experience frictional losses, such as those that might come from gear trains or surface-on-surface rubbing [11]. Oscillating systems—such as this bioreactor—are a common use for VCAs [10]. They are sold in a variety of shapes, sizes, and weights, so there would be little trouble finding one that could fit in the incubator. Two important parameters to consider in selecting a VCA are the force constant (how much force output is generated from 1A of current) and stroke (how far the magnet assembly can move). As with dimensions, VCAs come in a diversity of these properties. A VCA schematic can be seen in **Figure 1** below.

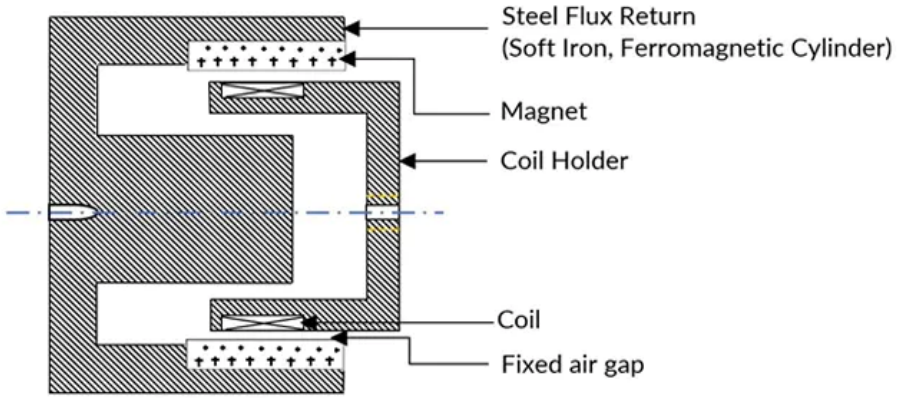

Figure 1. Diagram of a VCA with components labeled [12].

One clear downside of VCAs is their high cost. A single actuator for this application, depending on the dimensions, could cost between $500 and $1000+. Since one actuator per sample is required to ensure force control with cartilage's poroelastic creep behavior, this would become the largest area to dedicate the $5000 budget. Though theoretically, VCAs would fit all specifications, further investigation was made to mitigate the issue of cost.

Pneumatic Actuators.

The motion of pneumatic actuators comes from compressed air being fed through a port in an airtight chamber, which thrusts a piston in the chamber forward. A rod attached to the piston transfers the force outside the chamber. To return the piston to its original position, either a spring or a second port that is fed compressed air causes the piston to move in the opposite direction. An example pneumatic actuator can be seen in **Figure 2**. Instead of being electrically powered, pneumatic actuators are powered by an external compressed air tank.

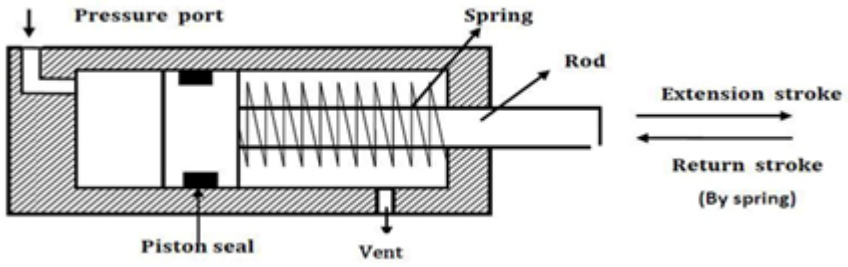

Figure 2. A general schematic illustrating how a spring-return actuator operates [13].

Pneumatic actuators are a good choice for situations where multiple actuators are required, as a single air tank can power multiple at once [13]. They also are cheaper than VCAs, in part because there are no electric components [14]. Whether they are more precise than VCAs differs from source to source [13], [14]. However, friction is generated between the piston seal and the pressure chamber. This creates losses that need to be accounted for during calibration. Even after mitigating this, long periods of operation would cause the piston seal to wear and the friction coefficient to change. Without a closed-loop control system that would give force readouts to a PID controller and modulate the pressure created in the chamber, this actuator would be subject to creep (especially at the high temperatures of the incubator) and lose the ability to output the correct force.

An additional consideration is whether the pneumatic actuator can resolve travel distances as small as is required by the bioreactor. In cartilage samples of 2 mm height experiencing 20% strain, the total displacement of the sample's upper face will be 0.4 mm. This means that a small amount of air that corresponds with moving the actuator 0.4 mm forward would need to be supplied each cycle. There are few pneumatic actuators on the market that have 0.4 mm within their stroke range, with the bottom of these ranges typically being much larger. Between frictional losses and stroke range limitations, moving forward with pneumatic actuation was decided against.

Hydrostatic Actuation.

A hydrostatic actuator is like a pneumatic actuator in the sense that they both generate force from controlling air pressure in a vacuum chamber. Instead of deflecting a rigid piston, though, a hydrostatic actuator deflects a flexible membrane that pushes the sample into a compressive interface. This mechanism can be seen in **Figure 3** below:

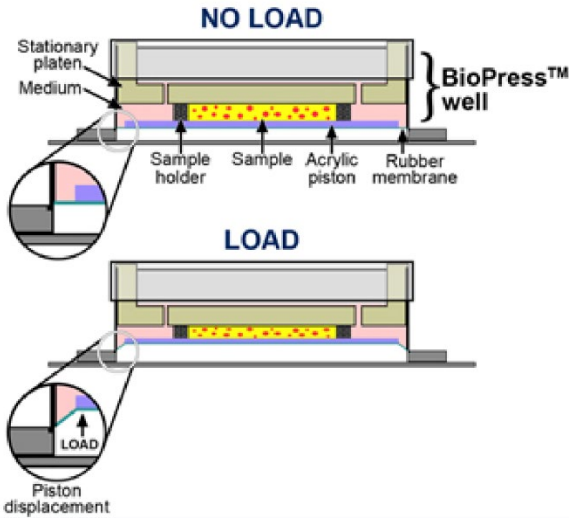

Figure 3. Flexcell's FX5000C compression system hydrostatic actuator in loaded and unloaded conditions [15]. Notice the membrane deflection in the circle on the left.

Force control is easily achieved here by control of membrane deflection. However, this system also has the issue of maintaining correct force output with sample creep. A closed-loop PID control system would be required to mitigate this, and this becomes expensive. Additionally, it cannot be guaranteed that membrane deflection would produce a uniform strain profile due to its elasticity. Sample holders and membrane edges as well as the air inlet would be specific locations of inhomogeneity in the strain profile. According to client specifications, the compression should be uniform. This rules hydrostatic actuation out of consideration.

After investigating these two mechanisms as well as others that did not end up showing as much promise, it became clear that the best way to achieve force control for the purposes of this project was with a VCA. Pneumatic or hydrostatic actuation would need a PID creep compensation system. This is not an issue with a VCA because a VCA will continue forward until it encounters a sufficient reaction force. In other words, the VCA will create 5.7N of force regardless of what is sandwiched between the magnet assembly and the compressive interface. This means that, as the sample exhibits poroelastic behavior and creeps, it will consistently experience the same 5.7N it did on day one of the experiment.

Actuator Product Selection

After selecting voice coil actuation as the mechanism to produce the force, the search for a product that fit the specifications could begin. There are a few key parameters that were highly relevant in selecting the proper VCA, as well as several design considerations that conversations with industry experts were able to provide over the phone. First, the parameters will be discussed, then the design considerations. This will lead to the VCA selection.

Parameters

Force constant [N/A]. The force constant is a measure of how much force the VCA will output when supplied with one amp of current. A high force constant is desired because that means

less power is required to operate the VCA and associated circuit. It is safer for the bioreactor operators to have minimized exposure to high voltage sources. Running the circuit at a lower power also means that it is less likely to fry.

Stroke [mm]. In any actuator, the stroke is the length at which the actuating arm extends during a cycle. In VCAs specifically, the stroke is how much the magnet assembly will displace from the coil when activated. If the stroke is too small, the desired deflection will not be fully created (though this is unlikely as it has been established that the deflection experienced by the samples will be around 0.4mm). If the stroke is too large, the small 0.4mm deflection may be too small to sufficiently resolve. The VCA could also be too large for the bioreactor if the stroke is too large.

Duty cycle [%]. In any circuit, the duty cycle measures for what percentage of the time the circuit is on versus off. While not expressly a property of VCAs, it was important to track potential actuator's performances at different duty cycles. The triangle wave circuit will have a duty cycle of 50%. If the circuit is later updated to something with a microcontroller, the duty cycle will be 100%. It is important that the VCA purchased operates successfully at both duty cycles at the temperature and humidity conditions in the incubator.

Maximum operating temperature [°C]. Due to the high temperature that the actuators will operate at, it is important to validate that the VCA can withstand this heat. According to the product design specifications, it must comfortably operate at 37°C.

Design Considerations

Horizontal translation. For a VCA to work, the coil and magnet assemblies cannot be attached. Products with a linear bearing down the center of the coil and magnet assemblies allow force to be generated along the axis without the coil bumping into the magnet. In VCAs without a linear bearing, additional reinforcements will be required to ensure that the movement is linear.

Tolerance. The typical tolerance in a VCA is about 10-15% of its force constant, according to the sales representative spoken to from Moticont Motion (a motion control company). This means that the force output may be different from actuator to actuator but should not change over the course of a single actuator's life in service. It is therefore possible to calibrate each actuator once they are ordered so that they produce the exact force output required. However, this means supplying each of the six VCAs with a slightly different current. This is doable but could make circuit design more challenging.

Magnet damage. Magnets used in VCAs create extremely precise force outputs as long as they aren't damaged. Damage could result from mishandling the voice coil or running it at too hot of a temperature. Damage should not result if the magnet experiences temperatures of less than 80°C. However, if a VCA is run at 100% duty cycle at near-maximum power in a 25°C environment, the coil would be ~120°C and the magnet would be ~80°C. Operating this VCA at incubator temperature (37°C) would damage the magnet. Therefore, sizing the VCA up so it doesn't run at maximum power will increase both the longevity and efficacy of the device.

Using these parameters and design considerations, four actuators from Moticont and one from ThorLabs were critically evaluated. A design matrix that details the deliberation can be found in **Appendix C**. In the end, the VCA from ThorLabs—VC125C/M—was selected. Specifications for VC125C/M can be found in **Table 1** below:

Table 1. Relevant design specifications for ThorLabs VC125C/M [16].

ThorLabs VC125C/M Specifications	
Force Constant	12.4 N/A
Stroke	12.7 mm
Coil Diameter	44.5 mm
Maximum Operating Temperature	230°F/110°C
Cost	$530.40
Linear Bearing?	No

The force constant is in an appropriate range and will be more efficiently powered than the other actuators. The stroke is 12.7mm, which should be small enough to resolve the force but large enough to be able to move the full extent of where the plunger needs to go between being on and off. This actuator is comfortably larger than the bare-bones specifications required, almost twice as large. This will help protect the magnet from heat damage. Confidence that it can withstand the heat is further inspired by the maximum operating temperature of 110C.

One downside with the selected VCA is cost. It costs $530 for one and ThorLabs does not offer any sort of unit discount on higher volume orders. Another downside is the possibility for horizontal translation. It will be very important to fix this, as the plunger goes through a narrow hole in the tray. Brushing up against the sides of the tray wall could create friction, which would decrease the precision of the force applied. Adding a flexure could resolve this and will be investigated next semester.

Overall, the ThorLabs VC125C/M satisfies all design specifications in theory. One VCA has been ordered, and as soon as it arrives, testing can begin to validate the specifications in practice. This will be a focus of early next semester.

Polytetrafluoroethylene (PTFE)

The bioreactor design utilizes VCAs to generate force. The force pushes the plunger and the sample containing a culture dish upward. A compressive pillar is used because it is necessary to counteract this force by applying compressive strain to the tissue. The material used for this pillar must be an appropriate interface material as it directly contacts cartilage tissue and media.

To find the interface material used in the bioreactor, several factors must be considered:

1. The material should withstand the warm and humid environment of the incubator. The bioreactor enters a culture incubator. It is typically maintained at 37°C and is a humid environment for cell cultivation, so the material must withstand this environment, and should not expand or deform due to temperature or humidity changes.

2. It must not be cytotoxic and should be chemically inert. As it directly contacts cartilage tissue and media, the interface material should not release or react with chemicals that could interfere with cell growth and proliferation during cultivation.
3. The material should be frictionless and not adversely affect the tissue sample due to the uniaxial compressive strain generated by the bioreactor. Mechanical compression-induced friction is a significant concern, and a material with a low friction coefficient is preferable to minimize the impact on the tissue.
4. The material must be sterilizable as it is used in tissue culture. Contamination of media and tissue in biological research is a severe issue, so the material should be able to withstand sterilization methods such as autoclaving at high temperatures and pressure.

Three materials were considered as candidates for the interface material: BioMed Clear Resin from FormLabs, Borosilicate glass (Pyrex), and Polytetrafluoroethylene (PTFE). BioMed Clear Resin, known for its biocompatibility and chemical inertness, is commonly used in cell and tissue culture research [17]. It also has a high melting temperature, allowing for sterilization through autoclaving, Ethylene Oxide, and gamma radiation [17]. However, BioMed Clear Resin is not frictionless and, crucially, is too expensive compared to other materials. Given the team's budget of $5000, and considering that much of it must be allocated to the VCAs, BioMed is not the ideal material.

Borosilicate glass, commonly known as Pyrex, is a material frequently seen not only in laboratories but also in kitchens. It is sturdy, has a high melting temperature, and can be easily sterilized using autoclave. Being chemically inert, it is commonly used in laboratories to store reagents [18]. However, for our specific use, the material has a significant drawback: it is challenging to fabricate. The fabrication of such hard glass requires specialized equipment, which is rarely available in companies or schools, and outsourcing the fabrication does not align with the goals of this design class. Therefore, Borosilicate glass was excluded from our material selection.

Although there were several material candidates, the material that met the design criteria was PTFE. PTFE is chemically inert, nontoxic, and nonflammable. It also has a low coefficient of friction, resulting in less shear stress on the tissue [19]. The material has high-temperature resistance with a melting temperature of 635°F (335°C), making it suitable for autoclaving without any issues [19]. Previous research supports its suitability for biological research, especially in tissue culture applications.

In summary, PTFE emerges as the clear choice for our design, offering a blend of essential characteristics that not only meet but exceed our criteria, ensuring a reliable and effective solution for our intended applications.

Fabrication Plan

PTFE will be purchased from McMaster-Carr. The company sells PTFE in the form of a rod, making it the best choice for our pillar design and eliminating the need to machine PTFE into a cylindrical shape for a pillar. The PTFE rod purchased from McMaster will be cut into six pieces using a band saw, and then the ends will be machined flat and smooth using a lathe. Additionally, a path for the screw will be created using a lathe and drill. The top plate will be precisely crafted using a mill to create six holes for attaching the PTFE pillars. The top plate and PTFE pillars will be fastened together using button head socket cap screws along with flat washers.

Electronics: General Concept

To drive a VCA, a circuit must be designed that can change current according to the specifications of the VCA. The general idea of the circuit will consist of an input source from a microcontroller or signal generator to produce the desired wave profile that feeds into a series of amplifier circuitry and then outputs into VCA. The general schematic of the circuit can be seen below in **Figure 4**. V1 represents the input source, U1 represents a power operational amplifier with R1 and C1 being interchangeable and variable according to the circuit needed, and V_{out} represents the output connection to the VCA. U1 needs to be a power operational amplifier as it needs to be able to output a high voltage and high current to drive the voice coil actuator at the desired force.

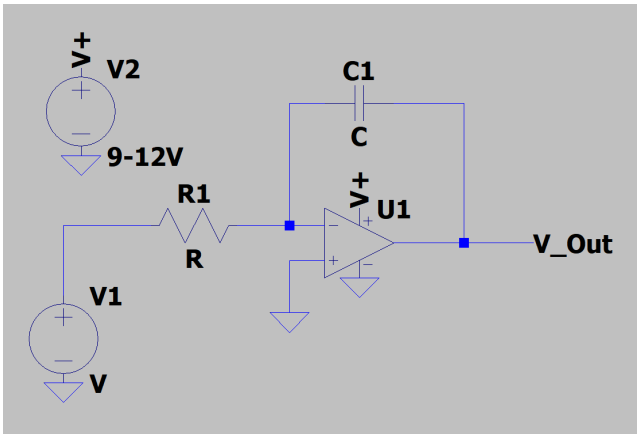

Figure 4. General circuit schematic to drive the voice coil.

The ideal wave profile would be similar to a modulus sine wave. This is shown in **Figure 5**. With that said, Dr. Henak would be open to accepting a triangular-like wave with a frequency output of 1Hz. This can be achieved in two ways. The first being directly using a signal generator or microcontroller to obtain a triangle or sine wave profile. The second would be using a DC supply from a wall adapter to power a series of amplifier circuitries. The wave profile and amplification can be effectively changed by changing the resistor and capacitor combinations on the amplifier circuitry.

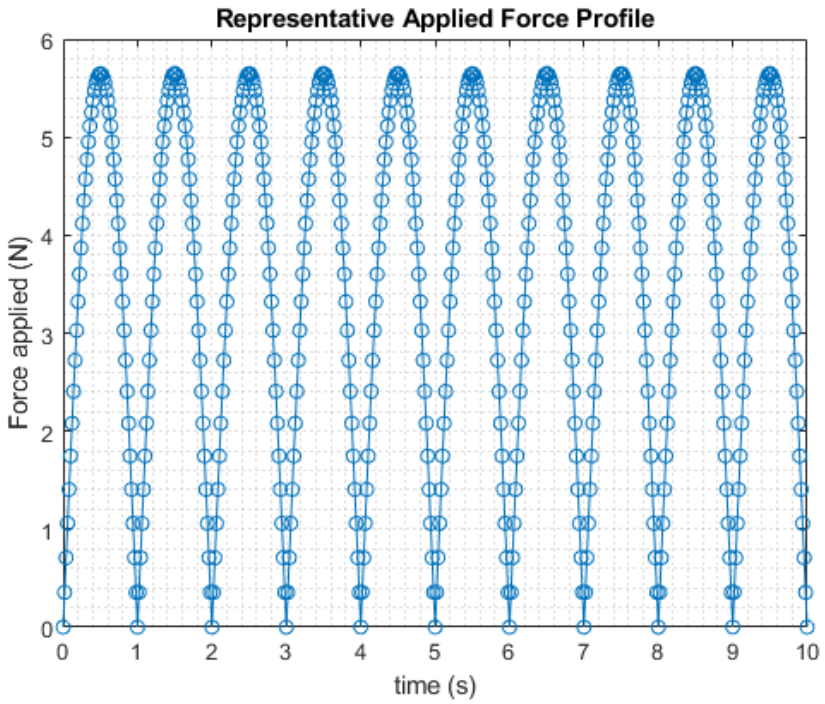

Figure 5. Ideal wave profile of a modulus sine wave.

Circuit Board

The initial idea on making a circuit that has a variable current or voltage depended on changing the resistor value through a programmable rheostat. This would effectively create a change in current which would drive the VCA. However, this method would be very tedious and require a lot of programming of the microcontroller. Varying current was then investigated as a solution. One method would be through an H-bridge where it acts like a transistor, switching the circuit on and off at a high frequency. The H-bridge would receive a DC input, where the H-bridge would output a sinusoidal wave. This method, however, would not be possible without a feedback loop from a load cell and a current regulator. Due to the nature of having a feedback loop and a load cell, the overall price of the electronics side would become increasingly costly. In addition, the programming and circuit setup would require a different housing design to accommodate the different positions each component will need to be. To tackle this problem, an in-house circuit board is therefore ideal as it is compact and has the possibility and capability of producing different wave profiles.

To make a circuit board that caters to our needs, the team worked closely with a professor from the biomedical engineering department, Dr. Amit Nimunkar, and a professor from the electrical engineering department, Dr. Mark Allie. Since Dr. Allie had a board in hand that can generate triangle waves, we decided to move forward using a DC adapter with different resistor-capacitor values. The triangle wave generator is soldered onto a PCB board using various components such as resistors, potentiometers, capacitors, and power amplifiers. The board is also powered through a wall adapter, capable of outputting up to 15V, instead of using a signal generator or microcontroller. This can be seen in **Figure 6** below with a different number of functions and resistors-capacitor combinations. The power input utilizes a wall adapter that outputs a peak DC voltage of 15V. Then by changing the resistor values, we can generate and output 9,

10, 11, and 12V, respectively. This can change by varying the resistor soldered on the PCB. Following that, we can effectively change the amplitude and frequency by changing the value of the potentiometer. The amplitude potentiometer can vary between 0-1V of the set DC value, and the frequency potentiometer is able to go as low as 0.1Hz, up to 20Hz. The output will be connected to the voice coil actuator, but as seen below, a resistor is hooked up for ease of testing.

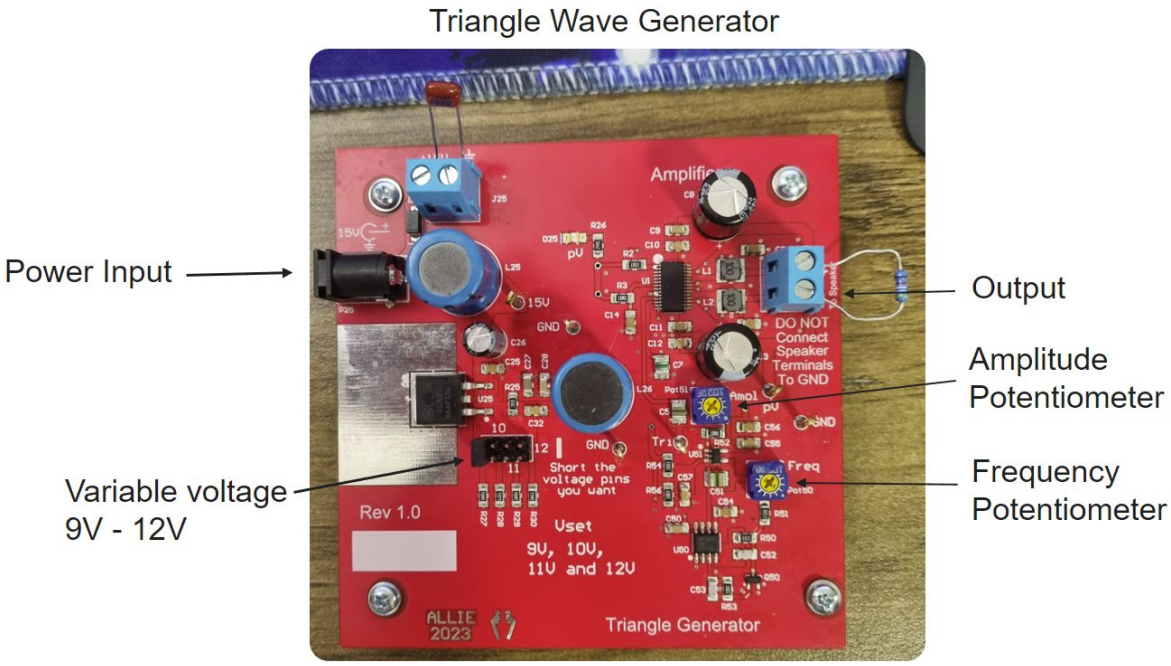

Figure 6. PCB board designed by Dr. Mark Allie.

Testing and Results

After testing the PCB board using an oscilloscope, the results obtained are shown below in **Figure 7**. It was noted that the wave profile is similar to that of a triangle wave but looks more like a capacitor's charging-discharging wave as the peaks are not sharp but smooth. It was also observed that the frequency of the wave is 2.63Hz with an amplitude of 8.73V.

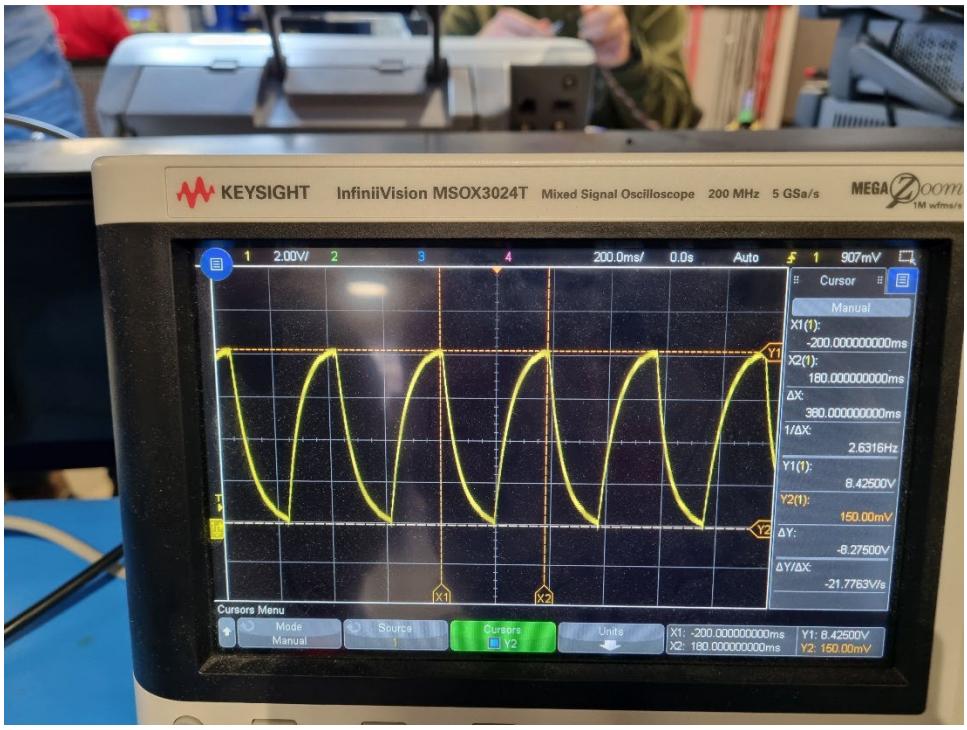

Figure 7. Wave profile observed when hooked up to oscilloscope.

While the frequency was within the requirements of 0.1-10Hz, we were not able to obtain a frequency lower than 2Hz as the circuit board automatically turns off below 2Hz. This is due to the safety feature built into the resistors and amplifiers to protect against any damage to the circuit components. To bypass this safety feature, an older model of resistors and amplifiers will need to be purchased and implemented to obtain a frequency of 1Hz.

Housing

With the actuating mechanism and device selected, a housing system could be developed that integrated all the bioreactor's components. Reexamining the exploded view of the prototype (**Figure 8** below) will provide an effective structure for illustrating the purpose of the housing's individual components.

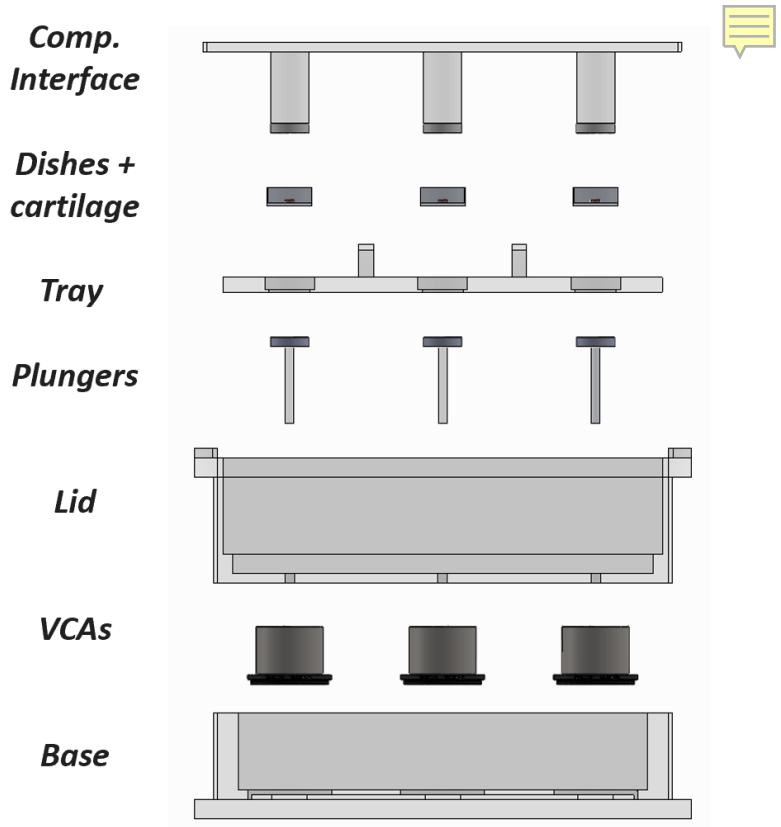

Figure 8. Exploded view of the bioreactor with its components labeled.

The housing base includes the actuators and electronics and is kept isolated from the rest of the bioreactor. This is to mitigate exposure to the humid bioreactor environment, as well as to isolate the electronics from the cartilage samples to minimize contamination. Future edits may be made to isolate the base more by adding a seal. The housing unit is the experimental chamber where the actuation will transpire. Future edits to the unit may involve opening up the sides to more freely interface with the humidity and to add holes for culture media replenishment.

The culture dishes which house cartilage samples rest in pits in a tray. The bottom of each pit has a cutout that is just wide enough for a plunger that is connected to the VCAs to pass through, connect with the underside of the culture dish, and propel it upward into the compressive interface. When the experiment is over, all samples can be removed easily at once by removing the compressive interface housing lid, grabbing the two handles on the sample tray, and lifting. Future edits will include a mechanism to latch down the compressive interface housing lid to prevent it from lifting off with actuation of the samples.

The housing will be 3D printed with Biomed Clear V1 resin, which is biocompatible. Even though nothing in the housing will touch the samples, it should still be ensured that exposure to contaminants is minimized.

Appendix F: Actuation Mechanism Design Matrix (ME 351)

To investigate the differences in the three actuator types that the team believed showed the most promise for creating the necessary force, a design matrix was made. Each actuator type—voice coil, pneumatic, and hydrostatic—was evaluated for cost, displacement, force output, force control, and general size and weight (footprint).

Voice Coil:

Cost	$520 / voice coil; not factoring in cost of current modulation/control
Displacement	12.7 mm stroke
Force	12.4 N/A force constant Peak continuous force: 15.5 N
(Force) Control	F = B x l – direct control over force input via Lorentz Force/Effect (i.e., current dictates for
Footprint	1.06 lbs; 2.2" base diameter

Summary: Excellent control over force; cost would limit number of samples. Approach validated in literature.

Pneumatic:

Cost	Waiting on quote – presumably far cheaper than voice coil due to constituent parts
Displacement	Customizable (12.5-300 mm)
Force	Reported linear relation between pressure & force: Push = DeltaP * 67.7; Pull = deltaP*60
(Force) Control	Air pressure regulation; need to compensate for frictional losses in shaft (~2% of force, according to company)
Footprint	~0.4 kg, depending on stroke; 14.3 mm base diameter

Summary: Control over force, given factor of friction (which would vary over time), would be difficult.

Hydrostatic:

Cost	Waiting on quote. Only one source of pressure control needed for membrane deflection, so presumably relatively inexpensive.
Displacement	Customizable (via changing deflection of membrane).
Force	Control via deltaP.
(Force) Control	Control over actuation is complex – requires accurate membrane deflection model in response to pressure change (which will also require modulation, similar to pneumatic). Attaching sample to flexible membrane could also be challenging.
Footprint	

Summary: Precise force control may be difficult, given variance in membrane deflection. Approach validated in literature & commercial application.

After examining how each actuator performed in each category, a definitive ranking emerged. Since proper force control is a high-priority specification, the VCA was selected despite the high cost.

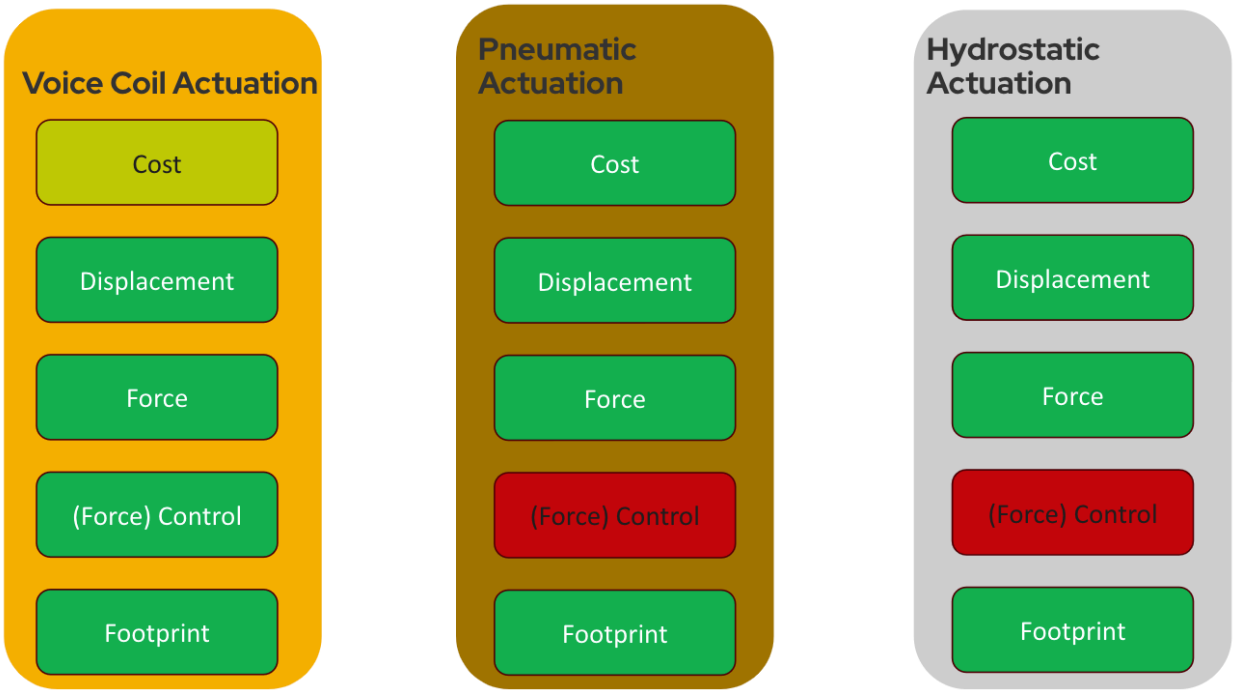

Appendix G: Actuator Product Design Matrix (ME 351)

After selecting VCA as the actuation mechanism, a product could be selected. Four from Moticont and one from ThorLabs were evaluated. The Moticont products were suggested by a Moticont engineer over the phone and are as follows:

1. GVCM-025-038-01: a standard VCA that should hit all specifications appropriately.
2. GVCM-051-025-01: a sized-up VCA that costs more but may be a safer choice.
3. LVCM-032-025-02: a VCA without the linear bearing that Moticont plans on launching as a GVCM model in the next month, would have to wait to order. Will have an output between options 1 and 2.
4. DDLM-038-051-01: a direct drive linear motor (DDLM) which is powered by VCAs.

These Moticont actuators were contrasted with the ThorLabs product that seemed to fit the specifications, VC125C/M. The actuators were evaluated on these five criteria:

1. Force constant: how little current we can use to power it
2. Degrees of freedom (if coil is fixed): "shaky" magnet assembly or not
3. Resistance to heat: high continuous force/larger
4. Availability: could we order it tomorrow
5. Cost: single order + five at a smaller unit price

The properties of each actuator were assigned a color based on a red-green scale that contrasted its value to the other products. The matrix is shown below:

	ThorLabs	Medium GVCM	Large GVCM	Small (G)LVCM	DDLM
FC	12.4 N/A	9 N/A	6.9 N/A	3.9 N/A	7 N/A
DoF	3	1	1	1	1
Heat Tol	324g / 13.5N	102g / 11N	320g / 23.5N	127g / 9.3N	280g / 14N
Availability	now	now	now	~1 month	now
Cost	$3120	$5101	$4972	~$5000	$3413

Even though the ThorLabs actuator will have issues with horizontal translation that will need to be rectified later, it is the cheapest and fits all the other specifications well. As such, it was selected for the bioreactor.

Appendix H: Arduino Code for H-Bridge Motor Controller

```
int motor1pin1 = 1;
int motor1pin2 = 2;

int motor2pin1 = 3;
int motor2pin2 = 4;

void setup() {
  // put your setup code here, to run once:
  pinMode(motor1pin1, OUTPUT);
  pinMode(motor1pin2, OUTPUT);
  pinMode(motor2pin1, OUTPUT);
  pinMode(motor2pin2, OUTPUT);

  pinMode(9, OUTPUT);
  pinMode(10, OUTPUT);
}

void loop() {
  // put your main code here, to run repeatedly:

  //Controlling speed (0 = off and 255 = max speed):
  // analogWrite(9, 100); //ENA pin
  analogWrite(10, 60); //ENB pin

  //Controlling spin direction of motors:
  digitalWrite(motor1pin1, HIGH);
  digitalWrite(motor1pin2, LOW);
```

```
  digitalWrite(motor2pin1, HIGH);
  digitalWrite(motor2pin2, LOW);
  delay(1000);

  digitalWrite(motor1pin1, LOW);
  digitalWrite(motor1pin2, HIGH);

  digitalWrite(motor2pin1, LOW);
  digitalWrite(motor2pin2, HIGH);
  delay(1000);
}
```

Appendix I: myDAQ Input Signal Generator LabVIEW VI

This is the front panel for the LabVIEW VI written for the myDAQ providing the input signal to the circuit. The VI is uploaded to the shared Box folder, located in the “Circuitry and Electronics” folder.

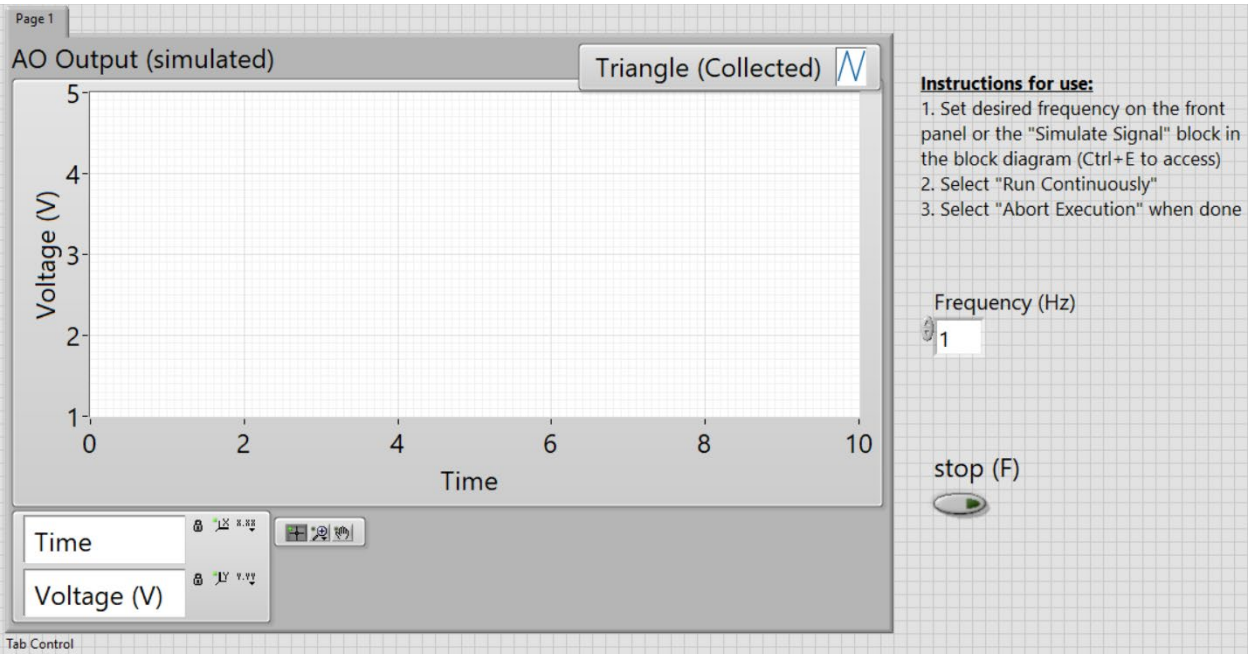

This is the block diagram for the LabVIEW VI written for the myDAQ providing the input signal to the circuit. The “DAQ Assistant” block will need to be updated when the NI USB-6001 is acquired because the VI was written for the NI myDAQ.

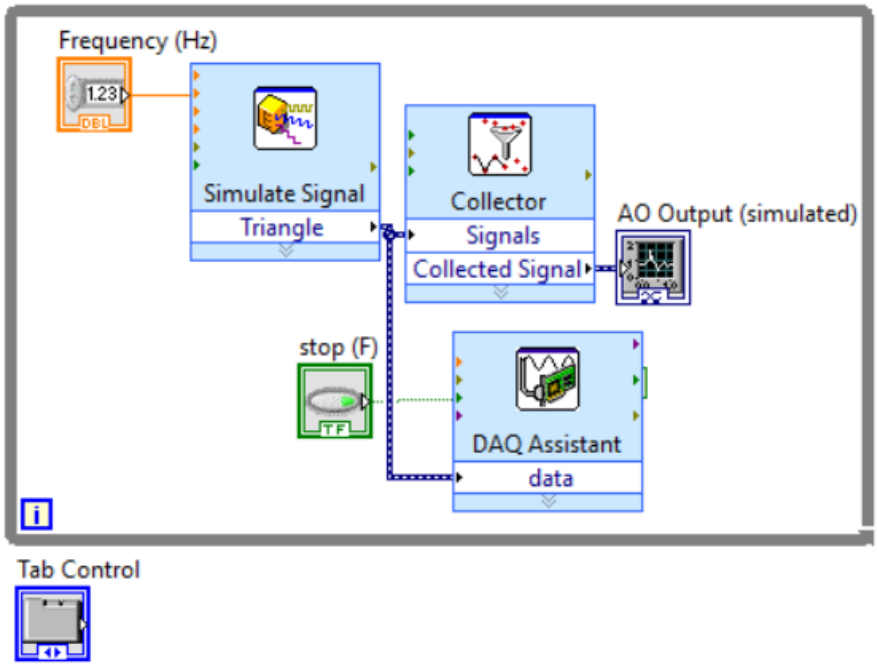

References

[1] E. Yelin, S. Weinstein, and T. King, "The burden of musculoskeletal diseases in the United States," *Semin. Arthritis Rheum.*, vol. 46, no. 3, pp. 259–260, Dec. 2016, doi: 10.1016/j.semarthrit.2016.07.013.

[2] Q. Yao *et al.*, "Osteoarthritis: pathogenic signaling pathways and therapeutic targets," *Signal Transduct. Target. Ther.*, vol. 8, no. 1, Art. no. 1, Feb. 2023, doi: 10.1038/s41392-023-01330-w.

[3] O.-M. Zahan, O. Serban, C. Gherman, and D. Fodor, "The evaluation of oxidative stress in osteoarthritis," *Med. Pharm. Rep.*, vol. 93, no. 1, pp. 12–22, Jan. 2020, doi: 10.15386/mpr-1422.

[4] S. K. Walsh, R. Soni, L. M. Arendt, M. C. Skala, and C. R. Henak, "Maturation- and degeneration-dependent articular cartilage metabolism via optical redox ratio imaging," *J. Orthop. Res.*, vol. 40, no. 8, pp. 1735–1743, 2022, doi: 10.1002/jor.25214.

[5] D. Kang *et al.*, "Selenophosphate synthetase 1 deficiency exacerbates osteoarthritis by dysregulating redox homeostasis," *Nat. Commun.*, vol. 13, no. 1, p. 779, Feb. 2022, doi: 10.1038/s41467-022-28385-7.

[6] S. K. Walsh, M. C. Skala, and C. R. Henak, "Real-time optical redox imaging of cartilage metabolic response to mechanical loading," *Osteoarthritis Cartilage*, vol. 27, no. 12, pp. 1841–1850, Dec. 2019, doi: 10.1016/j.joca.2019.08.004.

[7] M. H. Mohd Yunus, Y. Lee, A. Nordin, K. H. Chua, and R. Bt Hj Idrus, "Remodeling Osteoarthritic Articular Cartilage under Hypoxic Conditions," *Int. J. Mol. Sci.*, vol. 23, no. 10, p. 5356, May 2022, doi: 10.3390/ijms23105356.

[8] T. J. Lujan, K. M. Wirtz, C. S. Bahney, S. M. Madey, B. Johnstone, and M. Bottlang, "A novel bioreactor for the dynamic stimulation and mechanical evaluation of multiple tissue-engineered constructs," *Tissue Eng. Part C Methods*, vol. 17, no. 3, pp. 367–374, Mar. 2011, doi: 10.1089/ten.TEC.2010.0381.

[9] "CellScale Biomaterials Testing- Test Systems and Bioreactors." Accessed: Apr. 29, 2024. [Online]. Available: https://www.cellscale.com/

[10] M. Wilson, "What is a Voice Coil Actuator?," Machine Design. Accessed: Dec. 11, 2023. [Online]. Available: https://www.machinedesign.com/mechanical-motion-systems/article/21278883/tsn-fueled-automation-amps-up-the-ev-value-chain

[11] "Voice Coil Actuators." Accessed: Dec. 11, 2023. [Online]. Available: https://www.thorlabs.com

[12] H. Magnetech, "VOICE COIL ACTUATORS VS MOVING MAGNET ACTUATORS," Magnets By HSMAG. Accessed: Dec. 11, 2023. [Online]. Available: https://www.hsmagnets.com/blog/voice-coil-actuators-vs-moving-magnet-actuators/

[13] C. Dynamics, "How Pneumatic Actuators Work," Cowan Dynamics. Accessed: Dec. 11, 2023. [Online]. Available: https://www.cowandynamics.com/blog/how-pneumatic-actuators-work/

[14] SEMCOR, "How Pneumatic Actuators Work | Pneumatic Actuator Uses & Applications," SEMCOR. Accessed: Dec. 11, 2023. [Online]. Available: https://www.semcor.net/blog/advantages-of-pneumatic-actuators/

[15] "FX-5000C™ Compression System." Accessed: Dec. 11, 2023. [Online]. Available: https://flexcellint.com

[16] "Thorlabs - VC125C/M Voice Coil Actuator, 12.7 mm Travel, SM2 External Thread, Metric." Accessed: Dec. 11, 2023. [Online]. Available: https://www.thorlabs.com
[17] H. B. Musgrove, M. A. Catterton, and R. R. Pompano, "Applied tutorial for the design and fabrication of biomicrofluidic devices by resin 3D printing." bioRxiv, p. 2021.11.23.468853, Mar. 28, 2022. doi: 10.1101/2021.11.23.468853.
[18] M. Bengisu, "Borate glasses for scientific and industrial applications: a review," *J. Mater. Sci.*, vol. 51, no. 5, pp. 2199–2242, Mar. 2016, doi: 10.1007/s10853-015-9537-4.
[19] E. Dhanumalayan and G. M. Joshi, "Performance properties and applications of polytetrafluoroethylene (PTFE)—a review," *Adv. Compos. Hybrid Mater.*, vol. 1, no. 2, pp. 247–268, Jun. 2018, doi: 10.1007/s42114-018-0023-8.